12-2019

Examining the Effects of Greenland Ice Sheet Melting and Atlantic Meridional Shutdown on the Climate of Scandinavia and the British Isles

Tyler Lemburg
University of Nebraska--Lincoln, trlemburg@gmail.com

EXAMINING THE EFFECTS OF GREENLAND ICE SHEET MELTING AND ATLANTIC MERIDIONAL SHUTDOWN ON THE CLIMATE OF SCANDINAVIA AND THE BRITISH ISLES

by

Tyler Lemburg

A THESIS

Presented to the Faculty of

The Graduate College at the University of Nebraska

In Partial Fulfilment of Requirements

For the Degree of Master of Science

Major: Earth and Atmospheric Sciences

Under the Supervision of Professor Clinton M. Rowe

Lincoln, Nebraska

December, 2019

EXAMINING THE EFFECTS OF GREENLAND ICE SHEET MELTING AND ATLANTIC MERIDIONAL SHUTDOWN ON THE CLIMATE OF SCANDINAVIA AND THE BRITISH ISLES

Tyler Lemburg, M.S.

University of Nebraska, 2019

Advisor: Clinton M. Rowe

Earth's climate has been rapidly changing over the last hundred years, and its global average temperature is rising. However, climate change is far more complicated than a simple increase in temperature. For example, it is theorized that certain regions of Earth, including Scandinavia and the British Isles, could actually become cooler through ongoing climate change processes. Two of these processes are Greenland Ice Sheet (GrIS) melting, and slowdown of the Atlantic Meridional Overturning Circulation (AMOC). This research examines if climate change, through GrIS melting and AMOC slowdown, could contribute to cooler, instead of warmer, temperatures in Scandinavia and the British Isles.

The Weather Research and Forecasting climate model (WRF) was used to emulate a slowdown of AMOC via a widespread 5 K sea surface temperature decrease near the southern coast of Greenland. Although WRF contains a simple three-dimensional ocean model, this module was added relatively recently and was not used for this work. An experiment was run for a 1979-2009 time period over a domain covering Greenland, Scandinavia, and the British Isles, forced by the NCEP Climate Forecast System. Two runs were performed: a control run, and an experiment run including the sea surface temperature anomaly. The resulting climatologies showed a cooling of surface air temperature in Scandinavia and the British Isles of roughly 0.1 K for the experiment run compared to the control run, with a larger difference present in winter months. The anomaly's effects were also linked with the state of the North Atlantic Oscillation. Other differences between the two runs included a lower tropopause for the region, drier air in Scotland and Scandinavia, and varying regional

positive and negative differences of total precipitation and snow and ice, all again slightly more intense during colder months. It is surmised that GrIS melting and a slowdown of AMOC, when considered in isolation from other climate change effects, would lead to overall cooler conditions for Scandinavia and the British Isles.

ACKNOWLEDGMENTS

I would like to thank my thesis advisor, Dr. Clint Rowe, for providing his guidance during my graduate study as well as for working with me during my move to Georgia. Similarly, I would like to thank Dr. Mark Anderson and Dr. Steve Hu for their passion and encouragement as I began my meteorology studies and for serving on my thesis committee.

I would like to thank the Holland Computing Center at the University of Nebraska–Lincoln for providing the computing resources necessary to complete this research.

I would like to thank my colleagues throughout the Department of Earth and Atmospheric Sciences as well as my wonderful friends in the Department of Biology for their friendship and support.

I would like to thank my family for their support and in particular, I would like to thank my wife, Dr. Abigail Neyer, whose experience of the trials and challenges of graduate school was invaluable for my confidence and work ethic toward finishing my degree.

Contents

List of Figures

List of Tables

Chapter 1

Introduction

Climate modeling is a central study in the fields of meteorology and climatology. Starting with the development of one-dimensional models, the science of predicting Earth's future climate has advanced to develop numerous different three-dimensional climate models and parameterization schemes for those models. Applications of these models range from predicting the weather for a municipal area, to analyzing drought patterns and causes for a region, to examining effects of Milankovitch cycles on the planet's average temperature. However, one of the most important and impactful applications of climate modeling has been prediction of the effects of anthropogenic climate change.

The central factor of the climate change that has occurred during the 20th cenutry, and is projected to occur in the 21st century, is the warming of the planet due to the enhanced greenhouse effect due to accumulation of carbon dioxide in the atmosphere as a result of human activity (primarily the burning of fossil fuels) (IPCC, 2013). Hereafter this effect is referred to simply as the colloquial "climate change", even though the climate is technically always changing. Nearly all future global climate predictions include given scenarios for the expected amount of greenhouse gas (GHG) emission by humans and the effect of each of these scenarios on the global temperature. However, increases in GHG concentration and increases in global temperature affect other processes of Earth's atmosphere-ocean system.

For example, increased carbon dioxide leads to increased acidity in Earth's oceans, which not only affects the oceans' ecosystems but also the composition of the atmosphere should GHG concentration ever lessen. Another example is positive feedback of increased global temperature causing more Arctic and Antarctic ice melt, which also leads to higher sea levels and changes in Earth's albedo. Along with a warmer climate, climate change has been linked to more extreme weather and record-breaking storms. Since these changes are seemingly strange and random in nature, climate change has often been referred to as "global weirding" as opposed to "global warming" in news and popular science literature.

One effect of climate change which may be causing some "global weirding" is the melting of the Greenland Ice Sheet. Should the planet continue to warm at its current rate, it is possible the entire ice sheet, which sits atop Greenland, could melt within centuries. The input of this much freshwater to the oceans would have catastrophic consequences on sea levels which could greatly change the general circulation of the ocean and atmosphere. The general circulation (called the thermohaline circulation in the ocean) is responsible for transporting heat from the tropics, where insolation is greater, to the polar regions, which experience less insolation. Without the general circulation, regions near Earth's equator would be much hotter than they currently are, and polar regions would be much colder.

The objective of this thesis is to examine whether ongoing melting of the Greenland Ice Sheet imparts this "global weirding" for Scandinavia and the British Isles, making it cooler instead of warmer. This theory has previously been examined with global climate models by modeling the slowdown of the Atlantic Meridional Overturning Circulation (a portion of the thermohaline circulation), which could possibly be caused by the melting of the Greenland Ice Sheet (Frajka-Williams et al., 2016). The approach in this thesis, however, uses a regional climate model and emulates the slowdown of the Atlantic Meridional Overturning Circulation via a sea surface temperature anomaly. An experiment is run with two 30-year climate simulations, one as a control, the other with the anomaly. Each of these simulations outputs a 30-year climatology, and the differences between them show the effect that the

sea surface temperature anomaly, and thus Greenland Ice Sheet melting, could have on Scandinavia and the British Isles.

Chapter 2

Background

To understand how climate change will affect the climate of Scandinavia and the British Isles, we must examine the major processes which affect the climate of this region, beginning with the thermohaline circulation. The thermohaline circulation is a global oceanic circulation driven by tides, surface winds, and density, temperature, and salinity gradients. The thermohaline circulation generally consists of wind-driven currents which transport heat and water near the surface of the ocean, density-driven currents which transport heat and water closer to the bottom of the ocean, and areas of upwelling and downwelling between them. One major portion of this circulation consists of the Gulf Stream, a northward current along the eastern coast of North America. As tropical waters near the equator flow northward in the Atlantic Ocean, they become saltier and cooler through evaporation and sensible heat loss to the atmosphere, and sink to the southwest and southeast of Greenland to become North Atlantic Deep Water. The North Atlantic Deep Water then flows back southward in the deep ocean. The combination of the Gulf Stream, the area of North Atlantic Deep Water formation, and the deep ocean current returning these waters southward is called the Atlantic Meridional Overturning Circulation (AMOC) (Fig. 2.1).

Most of what we know about the Atlantic Meridional Overturning Circulation before the 21st century is constructed via models (Cheng et al., 2013). Observations on AMOC

did not begin in earnest until 2001 with an undersea observation array spanning the Atlantic Ocean at 26°N (Duchez et al., 2014). Other arrays soon followed (Frajka-Williams et al., 2019), in particular two that cross the northern Atlantic Ocean: one crosses the Labrador Sea between Greenland and North America, and the other spans from the southern tip of Greenland to Scotland. These make observations near the main areas of downwelling for AMOC between North America and Greenland, and between Greenland and the Norwegian Sea. While these observations have produced a wealth of *in situ* data, climate research strives to understand the time scales at which processes like AMOC might change. Unfortunately, we do not currently have the data necessary to accurately identify the decadal variability of AMOC. Still, it has been seen that AMOC's interannual variability in this century has exceeded that which has been reconstructed through climate models (Frajka-Williams et al., 2019).

Indeed, the variability of AMOC and its potential to slow or cease is a large part of research into global climate. Recent research has found that AMOC has been anomalously weaker during the last 150 years (Rahmstorf et al., 2015; Thornalley et al., 2018), and that it has weakened about 15% since the middle of the 20th century (Caesar et al., 2018). However, the modeling of AMOC is young; development of all the proper constraints and parameterizations of wind-driven components, positive and negative feedbacks, modes of equilibrium, etc., is ongoing. A complete shutdown of AMOC in the 21st century has been deemed "unlikely" by the Intergovernmental Panel on Climate Change (IPCC, 2013), however, further weakening of the circulation was evaluated as "very likely" (Liu et al., 2017).

The variability of AMOC need not be forced by any significant outside factor; in fact, AMOC has also been shown to be intrinsically variable without being forced (Danabasoglu et al., 2012). Several outside factors can influence the strength of AMOC as well. Any changes of temperature and salinity distributions in the ocean would affect the thermohaline circulation, and thus would affect AMOC as well. For example, AMOC has been found to

slow down because of an influx of freshwater from Arctic sea ice decline (Sévellec et al., 2017). However, there is another melting process which may greatly slow down AMOC: the melting of the Greenland Ice Sheet.

The Greenland Ice Sheet (GrIS) is the second-largest ice body on Earth, behind the Antarctic Ice Sheet. It covers 1,710,000 square kilometers, which is roughly 80% of the surface of Greenland. In general, it is more than 2 km thick with a maximum thickness over 3 km. GrIS also includes several glaciers and ice caps around its periphery which are separated from the main body of ice. Both GrIS and the Antarctic Ice Sheet have been drilled for ice cores, which provide proxies of past climate data. These proxies include carbon dioxide content of the air trapped in the ice, the thickness of layers in the ice, organisms trapped in the ice, and so on. While the detail and range of information from each of these proxies varies, altogether they have given climate researchers valuable data that reaches back 500,000 years.

Each year, Northern Hemisphere winter and summer seasons bring about a cycle of growth (accumulation) and decay (ablation) of GrIS. While there is almost always some ablation of the ice sheet throughout the year, in winter this ablation is generally less than summer and the ice sheet is able to grow as snowfall outpaces the melting. During the summer, ablation causes the ice sheet to shrink. However, due to globally increased temperatures from climate change, GrIS has experienced increased yearly melting since 1979 or earlier (Hassol, 2004). If the Greenland Ice Sheet were to melt entirely, it would cause a global sea level rise of 7.2 m; at the current rate of melting, this would take over 14,000 years to happen (Church et al., 2001). However, while the ice sheet waxes and wanes over millennia as Earth's climate shifts, the more abrupt changes in recent climate may cause an equally abrupt melting of GrIS. Climate models generally predict a warming of 3–9 K in Greenland for the 21st century. With those inputs, ice sheet models predict that the complete melting of the ice sheet could occur over centuries, not millennia (Hansen et al., 2007).

GrIS melting inhibits AMOC by freshening the salty water in the Labrador Sea and between Greenland and Iceland, decreasing its density and thus slowing down the sinking and formation of North Atlantic Deep Water. In turn, this slows down the entire AMOC (Frajka-Williams et al., 2016). Almost every study into AMOC's past, present, and/or future strength has examined its linkage with GrIS melting, yet conclusions vary as to the amount of influence GrIS melting exerts on AMOC's strength. Notably, however, the most comprehensive studies have theorized that AMOC strength will decrease by 18-37% from 2000 levels by the year 2100, and the impact of increased GrIS melting in IPCC AR4 and AR5 models has been mostly neglected (Blaschek et al., 2015; Bakker et al., 2016). Other studies find that GrIS melting enhances AMOC slowdown only if it provides a net freshwater gain south to the subpolar North Atlantic (Driesschaert et al., 2007; Hu et al., 2009; Yu et al., 2016), and they also find that the lost heat transport to the northern polar latitudes from this AMOC slowdown would be overcome by warming from climate change.

How does slowing of the Atlantic Meridional Overturning Circulation affect the climate of Scandinavia and the British Isles? Scandinavia and the British Isles lie between 50°N and 70°N latitude, similar to Canada and Russia. However, whereas Canada and Russia receive warm summers and cold, snow-filled winters, the climate of Scandinavia and the British Isles is more temperate and not liable to become as cool or snowy during winter (excepting more northern regions of Sweden and Norway). This is partly due to humidity from these locations' proximity to the ocean. However, AMOC also plays a role.

Earth's equator and the tropics receive more solar heating than the mid-latitudes and polar regions. This forces a general circulation in which heat is transported poleward from the equator. AMOC is a large part of Earth's ocean-atmosphere circulation (up to 25% of Earth's northward total heat transport (Bryden and Imawaki, 2001)) and it has been established that the heat transport AMOC provides from the tropics to the higher northern latitudes is responsible for the temperateness of the British Isles, Scandinavia, and the rest of the northwestern Europe relative to their latitudes (Rossby, 1996). While it is theorized

by some that the atmospheric circulation plays a larger role in the temperateness of the this region by an order of magnitude (Seager et al., 2002), the research in this thesis assumes that the role of AMOC in transporting heat to northwestern Europe is significant enough to warrant examination. We thus assume that should AMOC slow or shut down entirely, it could lead to cooler climates for this region. Indeed, over the last 40 years, the region of the Atlantic Ocean between Greenland and Iceland has cooled ~1 K whereas most of the rest of the planet has warmed by ~1 K, due to a century-long general slowing of AMOC (Bryden et al., 2005; Rahmstorf et al., 2015). Other research has solidified the link between AMOC slowdown and cooler climates for northwestern Europe. In fact, a strong freshening of the top layers of the North Atlantic causes a cooling for most of the Northern Hemisphere of 1–2 K, with the strongest response being around the North Atlantic (Vellinga and Wood, 2002).

Researchers have used global climate models to thoroughly quantify the effects of GrIS melting on AMOC and have associated varying degrees of AMOC slowdown for the next century with forecasted GrIS melting (Driesschaert et al., 2007; Hu et al., 2009; Blaschek et al., 2015; Bakker et al., 2016; Frajka-Williams et al., 2016; Yu et al., 2016). The exact methods and results vary, however, the general consensus is that AMOC saw an extraordinary slowdown during the 20th century and will continue to slow in the 21st century. The scope of this thesis, however, is not to specify changes or magnitudes of AMOC or GrIS melting, but instead to theorize what could become of the regional climates of Scandinavia and the British Isles should this process continue. While there have been many investigations into AMOC slowdown using global climate models, no research as of yet has examined how climate on a smaller scale will change if AMOC slowdown continues.

Since an AMOC slowdown will cause a lessening of northward heat transport in the Atlantic Ocean, and the melting of GrIS will inject cool, fresh water into AMOC's path, we choose to emulate the slowdown of AMOC by imposing an area of cooler sea surface temperatures on the southeastern coast of Greenland. While this method is not

prescriptive, as the true consequences of AMOC slowdown to sea surface temperature (as well as to atmospheric components) would be much more complicated, it serves well enough to investigate how a lessening of northward heat transport would affect the climate of Scandinavia and the British Isles.

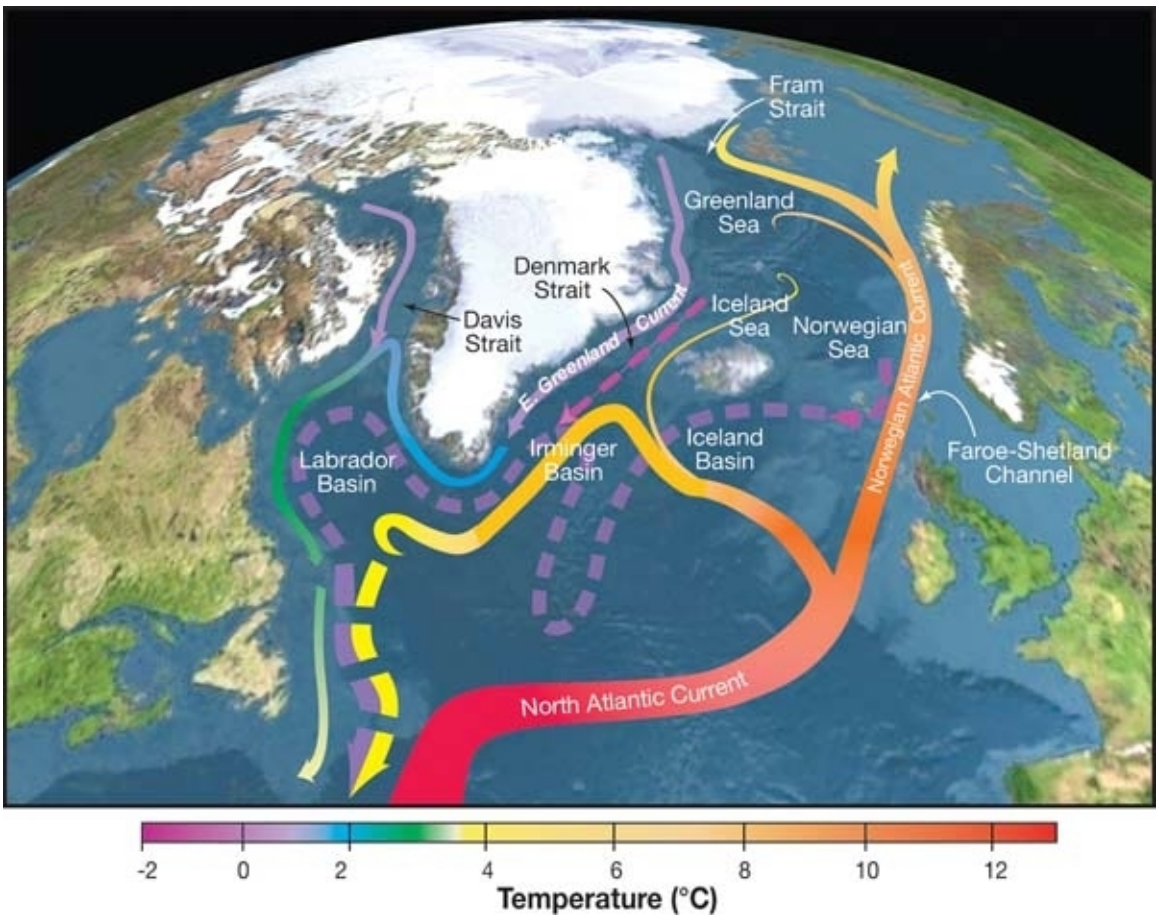

Figure 2.1: Diagram of the flows of the Atlantic Meridional Overturning Circulation. Waters from the Gulf Stream flow northeast across the Atlantic Ocean, become saltier and cooler, and sink near the coast of Greenland and elsewhere. From Curry, R. (2010)

Chapter 3

Data & Methods

Regional climate simulations were conducted to examine the effects of Greenland Ice Sheet (GrIS) melting on the climate of Scandinavia and the British Isles. Regional climate models produce output at higher resolution than global climate models, and give more detailed climatologies for the region in question. For this research, the Weather Research and Forecasting (WRF) model was used as a regional climate model. WRF is a next-generation mesoscale numerical weather prediction system designed for both atmospheric research and operational forecasting applications (Skamarock et al., 2008). In this application, WRF is sufficient to detail the linkages between GrIS melting and Northern European climate. WRF version 3.9.1 was the version used for this research, and was the latest version available at the time of this research.

3.1 WRF Domain and Forcing Data

WRF allows its users to specify custom domains and grid resolutions with nesting, if preferred. The domain for this research is an approximately 5000 km by 2600 km grid on a Lambert conic conformal projection, centered at 60°N, 15°W (Fig. 3.1). For this latitude, a Lambert projection provides the least distortion across a range of latitudes (the latitudes of intersection with the projection were set to 55°N and 65°N). The domain spans from

the Labrador Sea southwest of Greenland to the western edge of Poland, and contains the southern third of Greenland, as well as Iceland, the United Kingdom, Ireland, Norway, Sweden, Denmark, and the northern regions of Germany. The domain for this research has 27-km grid spacing, with 94 north-south grid points and 184 east-west grid points. No nested domains were included; adding a deeper level of resolution was both too time-consuming, as simulations would have taken over three times as long to complete, and not required for this application. A full specification of the options used to create the "geogrid" for WRF can be found in Table 3.1.

As with all regional climate models, WRF is forced on the boundaries of its domain by results from a model covering a larger domain containing the boundaries. These results could be from another regional climate model run at a larger scale, or from a global climate model. For this research, WRF was forced using data from the National Centers for Environmental Prediction (NCEP) Climate Forecast System (CFS) (Saha et al., 2010). The CFS is a fully-coupled global climate model, which models the interactions between Earth's atmosphere, land, oceans, and cryosphere. The original Climate Forecast System (CFS) is a global climate model that was developed by NCEP and released in 2004. Since then, NCEP has updated the model (now calling it CFS version 2 (CFSv2)) and, using the updated model, created a reanalysis dataset, the CFS Reanalysis (CFSR) (Saha et al., 2010). The CFSR dataset spans from 1979 to 2011; after March 2011, the data are separated and called the CFSv2 dataset. The CFSR output has 56-km grid point resolution; since this is less than three times the desired resolution for WRF in the model domain, the downscaling should succeed. WRF was run using the CFSR dataset with a "relaxation" of 4 grid points from the outside of the domain: grid points in this "relaxation" contain output that is a blend of the model output and forcing data.

Table 3.1: WRF Geogrid Options

&geogrid Option	Value
e_we	185
e_sn	95
dx	27 000 m
dy	27 000 m
map_proj	'lambert'
true_lat_1	55.00° N
true_lat_2	65.00° N
ref_lat	60.00
ref_lon	-15.00

3.2 WRF Simulations and Options

Simulations were run over a December 1979–November 2009 time period, with one month in November 1979 for spin up. This creates a 30-year climatology, which is standard for research of this type. A climatology beginning in December was chosen so that the typical seasons (December, Janurary, February (DJF), etc.) could be used for analysis and said seasons would all be contiguous. This research includes two simulations: a control run and an experiment run. The control run uses WRF to simulate the climate as given from the CFSR over the domain during the target time period; essentially, WRF downscales the CFSR output to the lateral boundaries for the domain and simulates inside the domain. The experiment run does the same, but the input data differ through imposing a seasonally invariant -5 K sea surface temperature (SST) anomaly near the coast of Greenland 3.1 in the input. This SST anomaly simulates the ocean's state if AMOC slows down and less warm water is brought into the higher latitudes.

WRF was run with the adaptive time step option when possible; at several times during the run, the adaptive time step caused the output to violate the Courant-Friedrichs-Lewy (CFL) condition. This occurs when the model produces a wave that travels through a gridpoint faster than the current time step. Thus, a static time step was implemented during

the latter half of each simulation to avoid these errors; time steps varied between 150–216 s. This option was calibrated so that output was still collected at regular intervals.

Since version 3.9, WRF comes bundled with pre-configured physics suites which represent well-tested options that work well together. Version 3.9.1 only contains two suites: “CONUS” and “tropical," designed for representing convective weather over the contiguous United States and convective weather at lower latitudes, respectively. For this application, a theoretical experiment running over 30 years, highly refined physics options decisions were not necessary to understand the impacts of an SST anomaly at this time scale. Thus, WRF was run using the “CONUS” physics suite option to most closely emulate the conditions of the North Atlantic. The “CONUS” physics suite utilizes the Rapid Radiative Transfer Model for GCM’s (general ciruclation models) (RRTMG) for shortwave and longwave physics. RRMTG is a correlated k-distribution band model which calculates the absorption and emission of radiation through the atmosphere. The “CONUS” suite uses the Thompson microphysics scheme, a 6-class scheme which computes the moisture tendencies of snow, cloud ice, water vapor, cloud droplets, graupel, and rain in the atmosphere. Other microphysics schemes utilize fewer classes of moisture and have different allocations of computation speed versus detail; the Thompson scheme strikes a balance of the two and is sophisticated yet computationally affordable. The “CONUS” physics suite also utilizes the Tiedtke cumulus parameterization, a mass-flux scheme with a shallow component and momentum transport, and the Mellor-Yamada-Janjic boundary layer parameterization.

At the surface, WRF’s “CONUS” suite uses the Mellor-Yamada-Janjic scheme for surface physics and the Noah Land Surface Model (LSM). The Noah LSM computes using four soil layers and handles frozen soil, partial snow cover, and ice sheets along with soil moisture and temperature. Urban physics parameterizations were turned off for this experiment; with 27 km grid spacing, few urban areas would resolve and the impacts of those that did would be limited. Boundary-layer physics parameterizations were called

every time step, while cumulus physics parameterizations were only called every 5 minutes of simulation time, and radiation parameterizations every 30 minutes.

WRF was run with the gravity wave drag option turned off. In WRF version 3.9.1, the inclusion of gravity wave drag requires minimal distortion of the east-west direction in the model domain. However, since this domain was a Lambert conic conformal domain at high latitudes, true east-west was too "twisted" from east-west of the domain grid for inclusion of this feature.

All other dynamics options were left at WRF defaults. These options include the base state temperature, set at 290 K, second-order diffusion computation, no damping, and positive-definite advection for moisture and scalars. Finally, the model was run in non-hydrostatic mode, to fully capture the effects of vertical momentum. A full list of relevant WRF runtime options to reproduce this work can be found in Tables 3.2 and 3.3.

Table 3.2: WRF Runtime Time Control and Dynamics Options

&time_control Option	Value
interval_seconds	21 600 s
history_interval	180 m
&dynamics Option	**Value**
w_damping	0
diff_opt	1
km_opt	4
diff_6th_opt	0
diff_6th_factor	0.12
base_temp	290 K
damp_opt	0
zdamp	5000 m
dampcoef	0.2
khdif	0
kvdif	0
non_hydrostatic	true
moist_adv_opt	1
scalar_adv_opt	1
gwd_opt	0

Table 3.3: WRF Runtime Domain and Boundary Options

&domains Option	Value
time_step	150 s
max_dom	1
e_we	185
e_sn	95
e_vert	30
p_top_requested	5000 Pa
num_metgrid_levels	38
num_metgrid_soil_levels	4
dx	27 000 m
dy	27 000 m
use_adaptive_time_step	true / false
step_to_output_time	true
target_cfl	1.2
max_step_increase_pct	5
starting_time_step	-1
max_time_step	-1
min_time_step	-1
adaptation_domain	-1
physics_suite	'CONUS'
radt	30
bldt	0
cudt	5
icloud	1
num_soil_layers	4
num_land_cat	21
sf_urban_physics	0
&bdy_control Option	**Value**
spec_bdy_width	5
spec_zone	1
relax_zone	4
specified	true
nested	false

3.3 Data Collection and Analysis

Typically in a climate modeling experiment such as the one presented here, researchers would validate the model by comparing the output of the control run with actual known

climate data from its time period. This establishes the bias of the model and this bias would then be utilized in other simulations to compute theoretical climate data. In this experiment, however, we did not compute the bias of the model. Firstly, with this experiment, there were no future simulations which needed to be corrected for the model bias. Secondly, although this model may be biased from the actual climate data from the 1979-2009 time period, we are only interested in the signal from the SST anomaly in isolation. Since we are comparing two climate simulations that are both biased, we can assume that their bias is equivalent and cancels out. Validating this model and applying its bias to climate simulations set in the future is outside the scope of this experiment.

WRF output was collected at 3-hour time intervals over the research time period. This output was used to first create averages and totals of various fields (e.g. average temperature, total precipitation, average wind) for each day, then those averages and totals were combined into monthly and seasonal averages and totals. Monthly totals were scaled to a 30-day month to account for differences in month lengths. For surface air temperature, snowfall, and total precipitation, monthly and seasonal averages and totals were then averaged across the 30-year time period to give monthly and seasonal averages for the entire climatology. All of these averages, variables, and totals were then compared between the control and experiment runs to observe the effects of the SST anomaly on the climate of Scandinavia and the British Isles.

Several different study regions in the model domain were analyzed to determine the effects of the anomaly. These study regions (which are not mutually exclusive) included Iceland, the United Kingdom, Scotland, Ireland, Sweden, Norway, western Norway (the western coast and mountain ranges of Norway, south of 63°N), and Denmark (Fig. 3.2). Regions were also grouped together to make other regions where they showed similar effects between the control and experiment runs. These groups were the UK and Ireland, and Sweden and Norway. Climatologies were computed in these regions by averaging each 3-hour output timestep of the WRF simulations and also averaging across all grid points

within the region. Similarly, climatologies for each season were computed by only using output timesteps from months within that season. Advection and moisture flux convergence were computed by calculating the instantaneous value of these variables at each of the 3-hour output timesteps, and then averaging across the 30-year run and across each region.

Standard deviations of values in the control run simulation were used to evaluate the scales of differences of surface air temperature, total precipitation, and snowfall between the experiment and control runs. For surface air temperature, the standard deviation was calculated using the average winter temperature for each of the 30 years in the simulation. Similarly, total winter precipitation and total yearly snowfall for each of the 30 years were used to calculate standard deviation for total precipitation and snowfall, respectively. Winter was chosen for surface air temperature and total precipitation because the effects of the SST anomaly in other seasons were less intense, and the analysis focuses mostly on effects of the SST anomaly during winter.

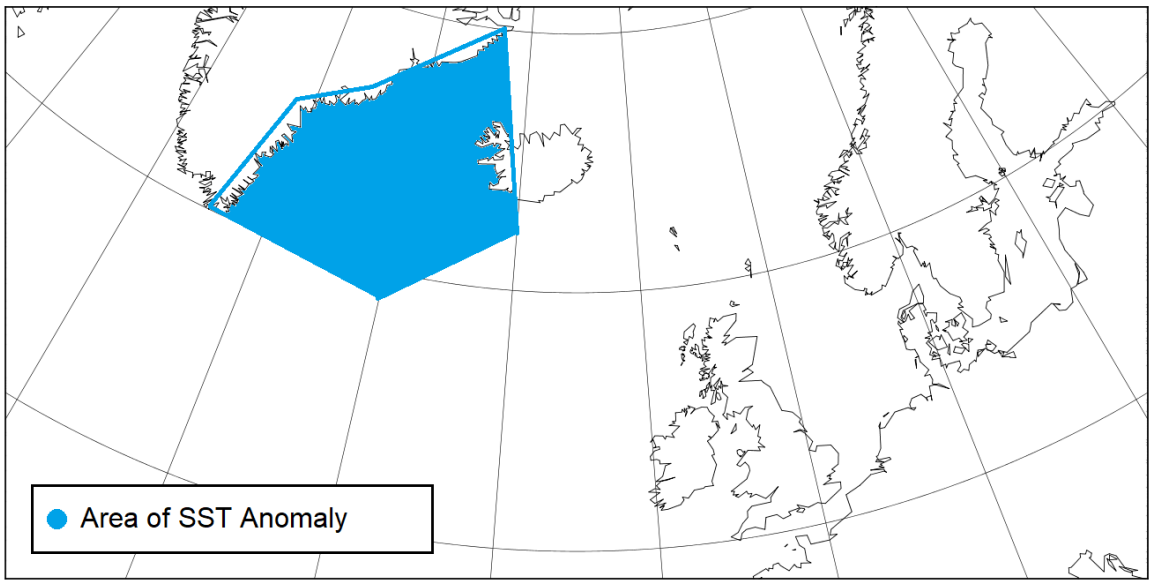

Figure 3.1: WRF model domain and region for the imposed −5 K SST anomaly. The SST anomaly was only imposed on oceanic data points in this region.

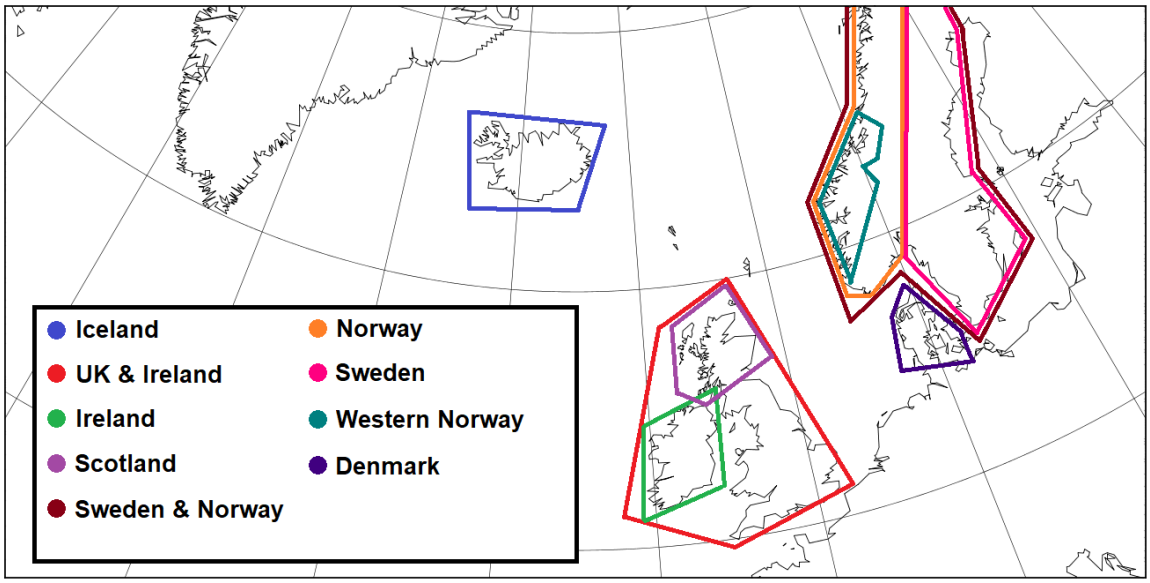

Figure 3.2: Various regions of Scandinavia and the British Isles were used for data collection and reporting. Data referring to a certain region is averaged horizontally over all data points inside that region's polygon on the above diagram.

Chapter 4

Results & Discussion

Throughout these results, scales were chosen in figures to best illustrate the magnitude of changes in the study regions of Scandinavia and the British Isles. In almost every part of the experiment, results at the imposed −5 K SST anomaly were more extreme than those downstream, however, the goal of this experiment is to derive the outcomes on downstream regions from imposing the SST anomaly, not to determine differences over the anomaly.

The main results of the experiment were as expected: imposing an anomaly of lower sea surface temperatures across a wide area over a 30-year time period led to a generally cooler climate near the anomaly and downstream of it. This cooler and drier air then forced a higher proportion of total precipitation as snowfall, a lower tropopause, and higher surface pressures and geopotential heights in those areas. While this cooler air in the experiment run contained less moisture content than that in the control run, the relative humidity was slightly higher, driving slight increases in total precipitation. Overall, the effects of the SST anomaly were found to be more pronounced during winter and early spring months; for example, in countries such as Sweden where the −5 K SST anomaly resulted in a decrease of ∼0.15 K in surface air temperature during winter months, this decrease was only 0.05 K at most during summer (Figs. 4.1–4.2). It stands to reason that due to the high latitude of the anomaly, with most of it lying above the 60°N parallel, its effects are mostly neutralized

during the summer months by the nearly full-time incoming shortwave radiation. For winter months, there is little external direct sunlight to the region, which allows the effects of the cooler surface waters to propagate. This is consistent with other patterns of weather and climate in the region. Thus, these results will focus almost exclusively on the effects of the SST anomaly and climate of the study regions during December, January, and February. When not specified in the text, values and descriptions of effects can be assumed to be for the winter season.

Of course, the scale of these effects is also dependent on the distance of the examined region from the anomaly, and the nature of the Earth's surface and atmosphere between the region and the anomaly. For example, effects of the anomaly in western Norway were significantly different than those found in eastern Norway, not only because western Norway is more mountainous but also because those mountains are between eastern Norway and the anomaly, which may hinder certain effects from reaching eastern Norway and Sweden. Iceland constitutes a special case of analysis in this experiment; with its proximity to the anomaly, and lack of unmodified ocean surface between it and the anomaly, it received the anomaly's effects in much greater magnitude. Surface air temperature, for example, decreased by over 1 K in Iceland for all months (Fig. 4.2).

4.1 Surface Conditions

With the -5 K SST anomaly imposed in the experiment run, surface air temperatures generally decreased across the study regions when compared to the control run (Fig. 4.3). Averaged across regions, this decrease was on the order of 0.1–0.2 K during the winter, and less than 0.05 K during the summer (Fig. 4.2). The temperature difference of a given grid point between the experiment run and the control run was dependent on the distance of the grid point from the anomaly; in winter months, the surface air temperature difference over oceans roughly forms a gradient outward from the anomaly. This temperature difference

was also amplified slightly over land, due to the lower specific heat of land as compared to the ocean (Fig. 4.3).

Comparing this temperature difference to typical variability among winters across regions illustrates the scale of the effect of the SST anomaly. In the UK and Ireland, the average temperature difference forced by the SST anomaly was about 16–23% of the standard deviation between average winter temperatures. In Sweden and Norway, this ratio was around 6–11%, and even smaller in Denmark (Table 4.1, Fig. 4.4). Since Iceland was adjacent to the sea surface temperature anomaly, the average temperature difference between runs was much larger compared to the standard deviation between average winter temperatures at about 225%. While the scale of this effect from the anomaly in Scandinavia and the British Isles is statistically small related to the differences between winters in these locations, it can be argued that the scale of this result is consistent with similar research. Research into effects of extreme GrIS melting and AMOC slowdown has shown that various scales of these effects would cause cooling for the entire Northern Hemisphere of 0.5–2.0 K (Vellinga and Wood, 2002; Hu et al., 2009), and these forcings are larger and wider than the SST anomaly applied in this experiment.

The nature of winds near where the anomaly was forced, and how those winds were affected by the anomaly, play a major role in how this temperature difference reaches Scandinavia and the British Isles. The average circulation near the southeastern coast of Greenland was found to be cyclonic at and below 850 hPa, with winds being stronger in the winter season than other seasons (Fig. 4.5). However, as can be expected, introducing a cold SST anomaly roughly in the middle of this average circulation also introduces a higher surface pressure, which weakens the cyclonic circulation (Fig. 4.6). At and below 850 hPa, wind speeds around this circulation were lessened by about one-third year-round in the experiment run, although the circulation was still cyclonic. A lessening of this circulation then weakens the westerly winds to the south of the anomaly, which bring warmer air off the warmer parts of AMOC over to Northern Europe. At higher pressure levels, this

effect is shifted slightly to the west, to be centered over the southern tip of Greenland, but the magnitude of the change as compared to the average circulation is negligible at and above 600 hPa (Fig. 4.7). Vertical winds were not appreciably changed by the anomaly: the average vertical wind component over the SST anomaly was about $0.001\,\mathrm{m\,s^{-1}}$ more downward between the surface and 850 hPa, with even smaller changes observed throughout the study regions.

Temperature advection at the surface was analyzed to further quantify the impact of winds on lower temperatures in the study regions. Advection was calculated by finding the advection at each three-hour time step of the WRF output, and averaging across the 30-year climatology. These calculations produce an estimate of the average instantaneous temperature advection for the entire 30-year period. The calculation of the gradients in these calculations led to slight amounts of noise being produced in the output. Thus, only values which significantly differed from this noise were considered.

During winter, surface air temperature advection in the control run was negative on the eastern coasts of the British Isles, ranging from values of -24 to $-18\,\mathrm{K\,day^{-1}}$, and positive on the western coasts, with values ranging from 18 to $24\,\mathrm{K\,day^{-1}}$ (Fig. 4.8). Over non-coastal areas, these values were smaller, with a maximum absolute value of $\sim 10\,\mathrm{K\,day^{-1}}$. This pattern is due to the general wind pattern of this region (see Fig. 4.6) blowing warmer air from the ocean onto land from the southwest, and blowing cooler air over land to the ocean on the northeast side. The pattern continues as the wind turns southerly and blows across western Norway; although temperature advection is negative on the southwestern coast of Norway, it is much more negative on the northwestern coast. As with the wind pattern, these coastal advection values are largest in the winter for this area and smaller in the other seasons.

Imposing the -5 K SST anomaly in the experiment run imparted a large change of advection near the anomaly and on Iceland, while changes for Scandiavia and the British Isles were minimal. The most significant change is a $1.0\,\mathrm{K\,day^{-1}}$ anomaly on the northwestern

coast of Scotland during winter (Fig. 4.8). The experiment run wind pattern did not significantly change winds across this area (Fig. 4.6), so the surface wind in the experiment run was southwesterly across northern Scotland. The increase of surface advection for this area is likely related to the difference between the surface air temperature in the experiment run, which is cooler than that of the control run, and the SST which is prescribed by the model input, and is the same for both runs.

The most interesting effect of advection changes for mainland areas of the study regions was on the southern areas of Norway (Fig. 4.8). The SST anomaly drove a surface air temperature advection difference of approximately $-0.5\,\mathrm{K\,day^{-1}}$ in this area, which certainly forced the negative surface air temperature difference for this region. Cooler air from the SST anomaly spread well into the North Sea between Scandinavia and the British Isles which would have then been advected over Norway via the southwesterly wind pattern here. However, these changes were on the order of 4–10% of the control run values, and it is difficult to definitively state that they are not results of or impacted by noise produced by the advection calculation algorithm. Thus, while the temperature advection in this case is worthy of analysis, the changes to the study regions (excepting Iceland) due to the SST anomaly are less significant next to other changes.

Changes in heat flux and water vapor content at the surface provide further linkages between the −5 K SST anomaly and the changing temperature in Northern Europe. Lower surface air temperatures over the anomaly led to cooler and thus drier air over and around the anomaly. During winter, the anomaly forced a large region of near-surface water vapor decrease of approximately $0.05–0.10\,\mathrm{g\,kg^{-1}}$ stretching east from the anomaly, over Iceland and throughout the Norwegian Sea (Fig. 4.9). However, outside the confines of the SST anomaly, the sea surface temperature was the same as the control run, since this variable was specified in the model input. Thus, drier air in the Norwegian Sea combined with the same sea surface temperatures as the control run led to a widespread increase in upward latent heat flux over this area during winter. That increase was $5–10\,\mathrm{W\,m^{-2}}$ (from values

of 50–105 W m^{-2} in the control run) (Fig. 4.10). This drier air at the surface extended over Scotland and western Norway during winter, but the change in latent heat flux above land in this case was negligible, as lower temperatures (along with increased precipitation, as discussed later) likely led to less evaporation.

Sensible heat flux change at the surface (Fig. 4.11) over the study regions had a pattern similar to the latent heat flux (Fig. 4.10). A large anomaly of downward sensible heat flux over the SST anomaly was observed, as heat would move from the warmer air into the cooler waters. This also contributed to a radiating gradient of more upward sensible heat flux downstream of the SST anomaly in the Norwegian Sea: as winds blow the air that lost some of its heat to the cool waters in the SST anomaly over warmer waters, more heat would transfer from the warmer water to the cooler air. The change of sensible heat flux during winter was on the same order as the change in latent heat flux, with increases of 5–10 W m^{-2}, from values of 30–50 W m^{-2} in the control during the winter (Fig. 4.11). However, combined with the latent heat flux, this warming was not sufficient to offset the cooling driven by the cooler air from over the anomaly, as surface air temperatures over this area were still lower in the experiment run by 0.1–0.3 K (Fig. 4.2). Over land, sensible heat flux change at the surface was on the order of less than 1 W m^{-2} in most areas.

Another factor that influenced the change in Northern European climate due to the SST anomaly was the North Atlantic Oscillation (NAO). The NAO is an oscillation between modes of surface pressure differences of two zones in the North Atlantic: the Icelandic Low, a persistent low pressure system situated over Iceland (and essentially where the SST anomaly was imposed) and the Azores High, a persistent high pressure system centered in the Atlantic Ocean west of Spain (Wallace and Hobbs, 2006). The NAO index is quantified by the difference of surface pressure between these two systems. When the index is positive (NAO+), the differences in surface pressures and strength of these two systems increase the westerly winds that drive air from New England across the Atlantic Ocean into Northern Europe. This generally leads to increased atmospheric moisture being brought into the

region through evaporation as these winds blow over the Atlantic Ocean, which leads to cooler summers, milder winters, and more precipitation and storms on average. When the index is negative (NAO-), the differences between the surface pressures of these two zones are less, and the westerlies into Northern Europe are less powerful. In general, this causes more of the moisture brought in via these winds to be instead circulated around the Azores High, and storms and precipitation will instead track into Spain instead of Scandinavia and the British Isles.

In the experiment run, lower surface air temperatures over the study area, particularly over the British Isles and western Norway, were found to correlate with positive values of the historical NAO index (Figs. 4.12–4.13). Stronger westerly winds from NAO+ would bring the cooler surface air of the SST anomaly over to the British Isles and Scandinavia more strongly, and thus create lower surface air temperatures. As discussed earlier, this cooling would be somewhat offset by the sensible and latent heat flux from the ocean between the SST anomaly and the study area, however, the cooler air remained the stronger force. This correlation was found to be stronger in the winter in the UK and Ireland region (Fig. 4.12). Weaker correlations were found between the NAO index and lower surface air temperatures in the other study regions (Table 4.2), with winter having a stronger correlation than the other seasons as well. Although this correlation is stronger in winter, it is still quite weak ($R^2 = 0.178$ for Scotland is the highest R^2 value outside of Iceland). We note that this correlation, while expected from the effects of NAO and visually verifiable via our data, is not statistically significant in this climatology.

It should be noted that the values of NAO index in the experiment run could be different than actual historical values used for the correlation. NAO values in the experiment run would be impossible to compute without extending the domain to also cover Portugal, Spain, and the Azores. Although a high surface pressure anomaly near Iceland would exist in the experiment run, which, aside from any other influence would lessen the NAO index, it is reasonable to assume that the atmosphere as a whole would soften any NAO change

from the SST anomaly. Thus, correlation with the historical NAO values serves for this application.

4.2 Temperature above 850 hPa

Above the lower portion of the troposphere, temperature changes due to the imposed SST anomaly were minimal. From the surface to about 500 hPa, air temperature across the domain of the simulation was found to be about 0.05–0.25 K lower in the winter due to the −5 K SST anomaly, with cooler areas found directly over the anomaly (Fig. 4.14). From 400 hPa to 150 hPa, however, a warming of the upper-level air of 0.025–0.200 K is found in the experiment run due to the SST anomaly (Fig. 4.14). This could be due to a slight lowering of the tropopause across the region; cooler surface air would tend to lower the tropopause. However, there was no meaningful way from the results to calculate an amount the tropopause was lowered. Average winter lapse rates were calculated for Aberdeen, Scotland, as an example. At the grid point nearest Aberdeen, average lapse rates during winter for the control and experiment runs were both larger than $6.5\,\mathrm{K\,km^{-1}}$ at 300 hPa then decreased to $\sim 1.75\,\mathrm{K\,km^{-1}}$ between 250 hPa and 200 hPa. It can be assumed that the tropopause above Aberdeen lies at about 250 hPa during winter and its change is on the order of a few hPa at most, having little effect on conditions at the surface.

The only exception to this warming at height was over the southern tip of Greenland. A decrease in temperature was observed above this area from 400 hPa to 150 hPa, of ∼0.05 K, during winter (Fig. 4.14). Between 500 hPa and 200 hPa, winds above the southeastern coast of Greenland were found to be influenced by the anomaly. Winds were generally southwesterly on the order of $10\,\mathrm{m\,s^{-1}}$ at 400 hPa in the control run, but in the experiment run, winds were $1\,\mathrm{m\,s^{-1}}$ more northwesterly (Fig. 4.7). In fact, at and above 700 hPa, the change in average winds due to the SST anomaly was cyclonic over the southern tip of Greenland (Fig. 4.7). This is not to say that average winds in either run indicated a high

pressure center in this area; in the experiment run, winds were still generally westerly, although both runs include different behavior on the mountains of Greenland, where wind runs more southwesterly. However, this cyclonic wind anomaly could be contributing to the lower temperatures lying adjacent to the warmer ones at height as observed in the difference between the experiment run and the control run.

4.3 Total Precipitation

Changes to total precipitation between the control run and the experiment run were varied. While it was found that the aforementioned cooler air from the -5 K SST anomaly created a large decrease in total precipitation at the anomaly and over Iceland during the winter and spring months, this signal did not propagate cleanly to Scandinavia and the British Isles (Fig. 4.15). We can expect that some of this change is a result of precipitation being somewhat stochastic as a process, but there are still several interesting points to be made about the output of these simulations. Total precipitation is given as the liquid equivalent of the combination of all forms of precipitation.

For example, Scotland received an average increase of 0.43 cm of precipitation for each winter in the experiment run as opposed to the control run. However, western Norway received 0.20 cm less precipitation on average each winter in the experiment run as compared to the control run. Some of this difference is likely due to a downstream effect from the extra upward latent heat flux occurring in the Norwegian Sea. It is possible that as this process works to offset the lost heat in the air above the Norwegian Sea from the SST anomaly, and more water vapor enters the air, the lower average air temperature is also causing that vapor to precipitate downstream. Indeed, although absolute water vapor content decreased across the region, the drop in temperature was sufficient to actually increase the relative humidity in the experiment run (Fig. 4.16). This increase was strongest in Scotland and western Norway, each with average increases of ~0.6 %.

Why then does western Norway not receive an increase in precipitation? Although both of these regions are mountainous, western Norway's mountains are much higher than Scotland's (highest at ~2400 m as opposed to ~1300 m), and western Norway's mountain range forms more of a barrier running north-south against the Norwegian Sea, whereas the mountains of Scotland do not. In essence, the extra uptake of moisture would not make it high enough to overcome the barrier produced by Norway's mountains, whereas it would easily navigate around the topography of Scotland.

This theory can be further examined by evaluating the moisture flux convergence. Moisture flux convergence was integrated from 1000 hPa to 100 hPa at each timestep in the simulation output, and averaged to provide an average for the entire run. In the control run, moisture diverged slightly from land regions during winter on average (Fig. 4.17). In the experiment run, we observe few meaningful changes to moisture flux convergence in the study area. The moisture flux convergence difference shows moisture diverging from the region of the SST anomaly. Noise from the moisture flux convergence computation forms the remainder of the data; as with the advection calculations, gradient computation introduces these bands of noise in the output. Due to this noise, it is impossible to gain any meaningful conclusions from the moisture flux convergence anomaly over the study regions: changes were on the order of 10% of the control run values but not in any sort of pattern or concentrated region beyond the SST anomaly and the Norwegian sea as described above.

When comparing the differences in total precipitation to the standard deviation of total precipitation between winters in the control run, however, we see that the increase in winter total precipitation for Scotland was somewhat minimal. The average increase for Scotland was only 19% of the standard deviation of total precipitation between winters (Fig. 4.18). Most of this increase was actually in the form of snow and ice, as discussed later.

Regions that were "protected" from the anomaly by distance or topography, such as England, Sweden, and Denmark, received less precipitation on average during the winter in

the experiment run as compared to the control run. This decrease was only around 0.1 cm averaged across each of these regions, from values between 7 cm and 15 cm. The effect of any extra moisture uptake from the Norwegian Sea would have been spent over nearer land areas or over the sea itself.

4.4 Snowfall

Imposing the −5 K SST anomaly caused a variety of effects on snowfall for the simulation domain and the study regions. Generally, mountainous parts of the study regions that were closer to the anomaly received about 0.1 cm more liquid equivalent of snow and ice during each of the winter months on average (Fig. 4.19). While there was no additional moisture flux converging into the study regions in the experiment run and total precipitation decreased as compared to the control run, lower average temperatures across the study regions imply that more of the precipitation that did fall in the experiment run would be as snow and ice instead of rain.

Of course, the addition of a millimeter of snow per month would hardly be noticeable from a personal perspective, but since that value is averaged across an entire country or region, it implies that there is a significantly larger amount of moisture being precipitated as snow. In fact, the UK and Ireland received 10-20% more snow and ice per year on average in the experiment run, from values of less than 7.5 cm liquid equivalent of snow and ice per year in the control run (albeit from much higher values in Scotland) (Fig. 4.20). For Sweden and Norway, the increase due to the anomaly was closer to 5%, with localized decreases. This change was from values ranging from 20–40 cm liquid equivalent of snow and ice per year in the control run for Sweden, and 40–100 cm and higher liquid equivalent of snow and ice per year for Norway.

Further, differences in total yearly snowfall caused by the −5 K SST anomaly were more significant when compared to the standard deviation than temperature and total precipitation.

For Scotland, the increase to yearly snowfall was about 60% of the standard deviation of snowfall between each year (Fig. 4.21). Western Norway and other parts of the UK & Ireland also received increases of between 10–40% of their standard deviations of yearly snowfall. Altogether, the effects of the SST anomaly on snowfall for Scotland would likely be the most noticeable of any effects in this research. With Scotland's proximity to the SST anomaly and the ocean, its relatively large temperature change between runs, and the general humidity of the region, it makes sense that it would experience a larger amount of its total precipitation as snowfall and that this increase would be more to scale of the variability of yearly snowfall, compared to other regions in the study.

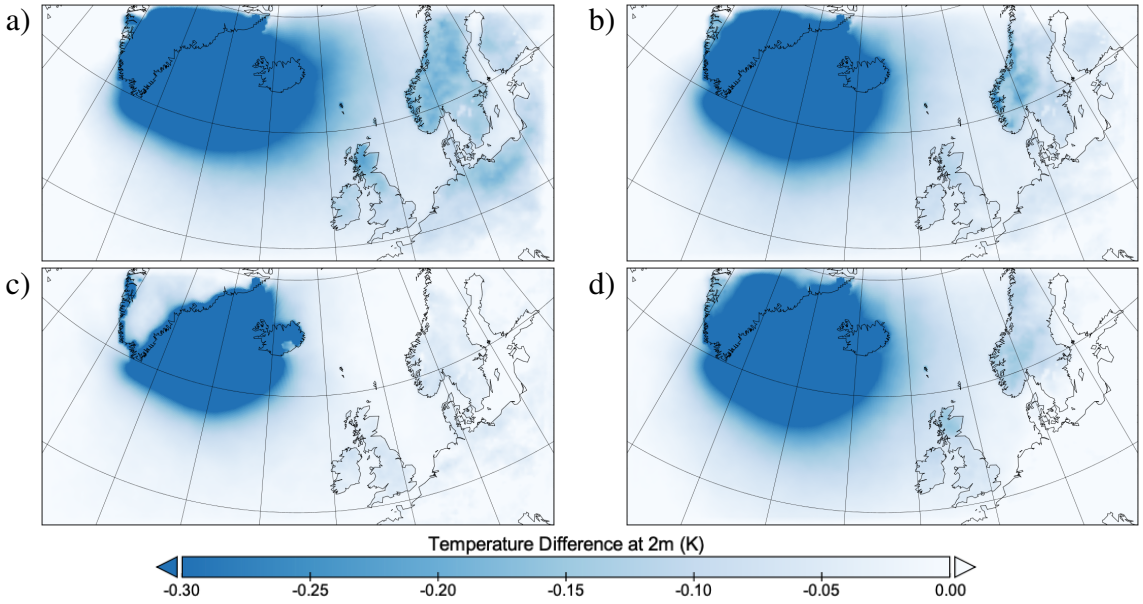

Figure 4.1: Temperature difference between experiment and control runs at 2 m, averaged seasonally for a) winter, b) spring, c) summer, and d) autumn. Scales chosen to show detail over Scandinavia and British Isles.

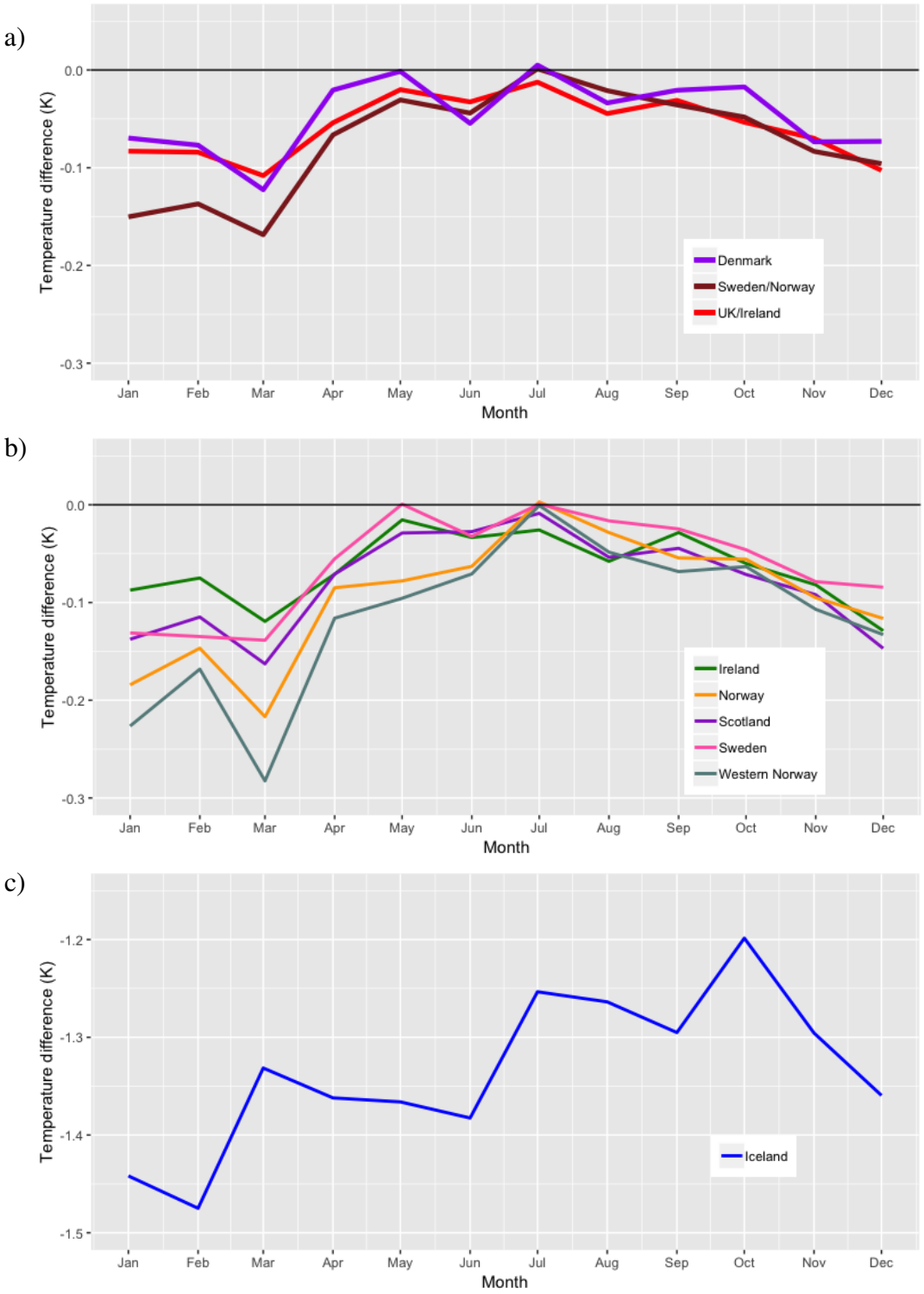

Figure 4.2: Average surface air temperature difference between experiment and control runs across a) grouped and larger regions, b) smaller regions, and c) Iceland, averaged by month. Note the different scale for c), as Iceland was much cooler comparatively than other regions due to its proximity to the SST anomaly.

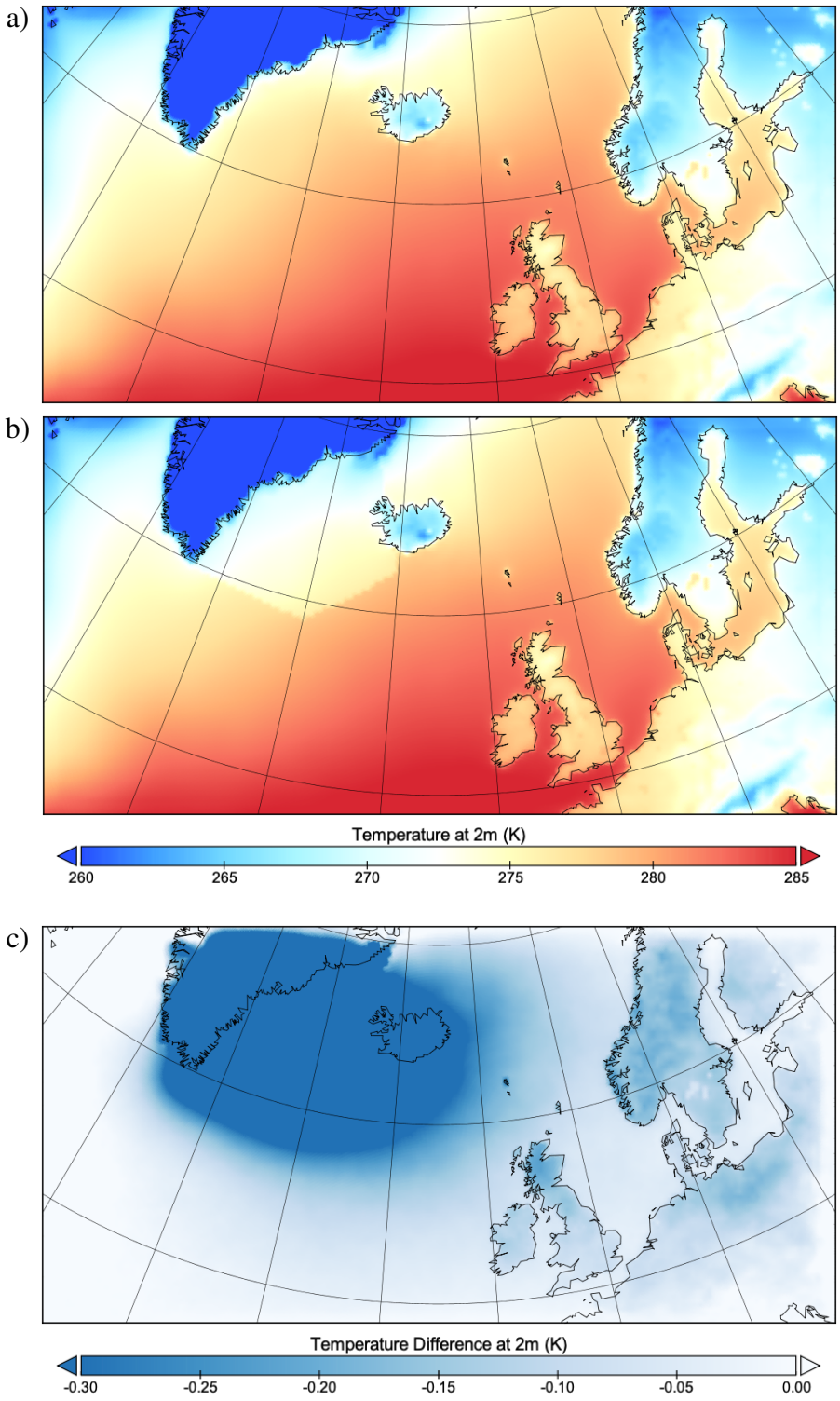

Figure 4.3: (a) Average winter air temperature at 2 m for control run. (b) Average winter air temperature at 2 m for experiment run. (c) Surface temperature difference between experiment and control runs at 2 m, averaged seasonally for winter. Surface air temperature over anomaly approaches −5 K. Scales chosen to show detail over Scandinavia and British Isles.

Table 4.1: Average winter temperature difference between experiment run and control run, standard deviation between average winter temperatures in control run, and ratio between the temperature difference and the standard deviation, for each study region.

Region	Difference (K)	Standard Deviation (K)	Ratio
Iceland	-1.424	0.632	-2.253
UK & Ireland	-0.090	0.536	-0.168
Ireland	-0.098	0.595	-0.165
Scotland	-0.134	0.589	-0.228
Sweden & Norway	-0.127	1.706	-0.074
Norway	-0.149	1.716	-0.087
Sweden	-0.116	1.809	-0.064
Western Norway	-0.176	1.602	-0.110
Denmark	-0.073	1.343	-0.054

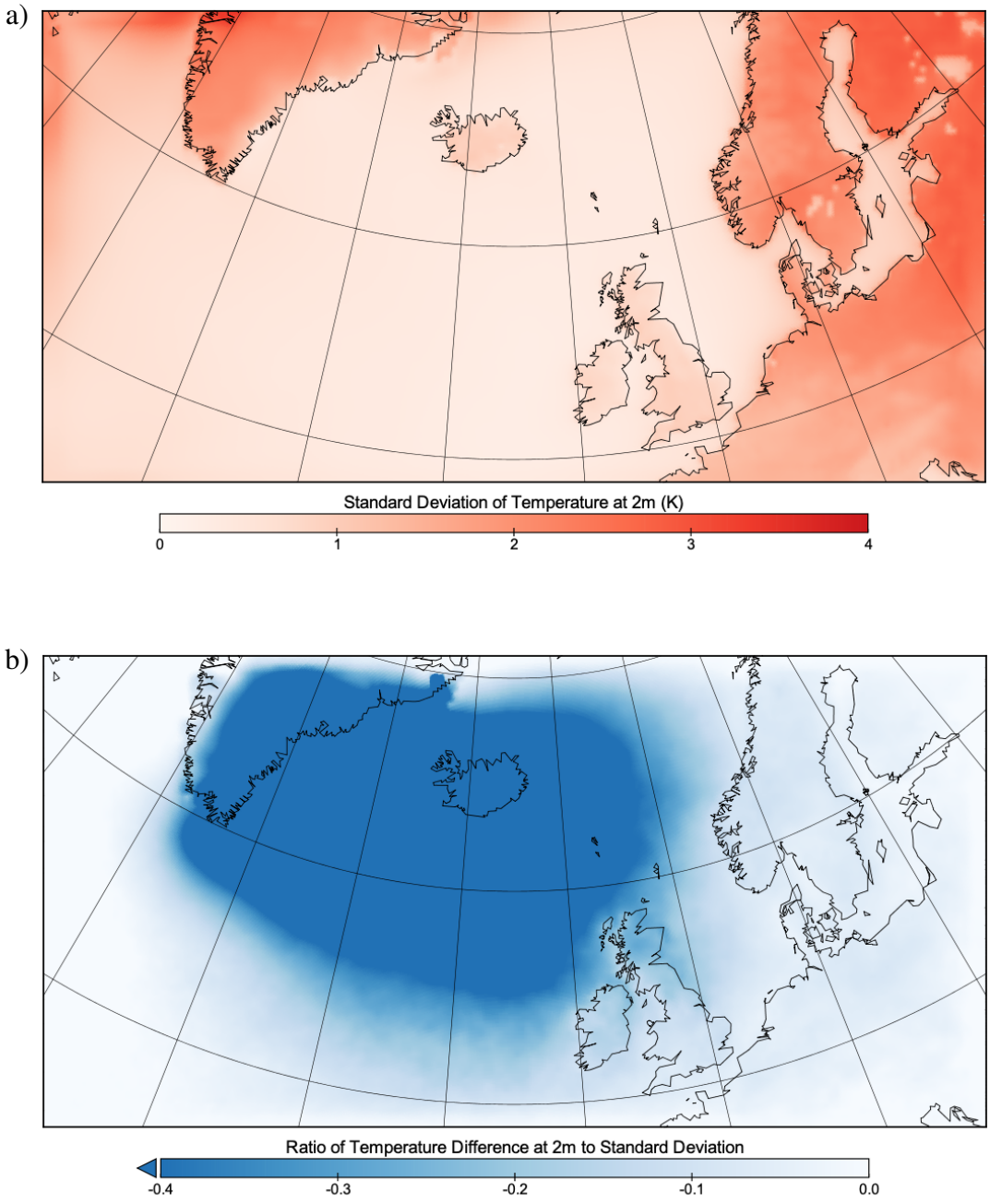

Figure 4.4: (a) Standard deviation between average winter surface air temperature for each year in control run. (b) Ratio of surface air temperature difference to standard deviation between average winter surface air temperature. Scales chosen to show detail over Scandinavia and British Isles.

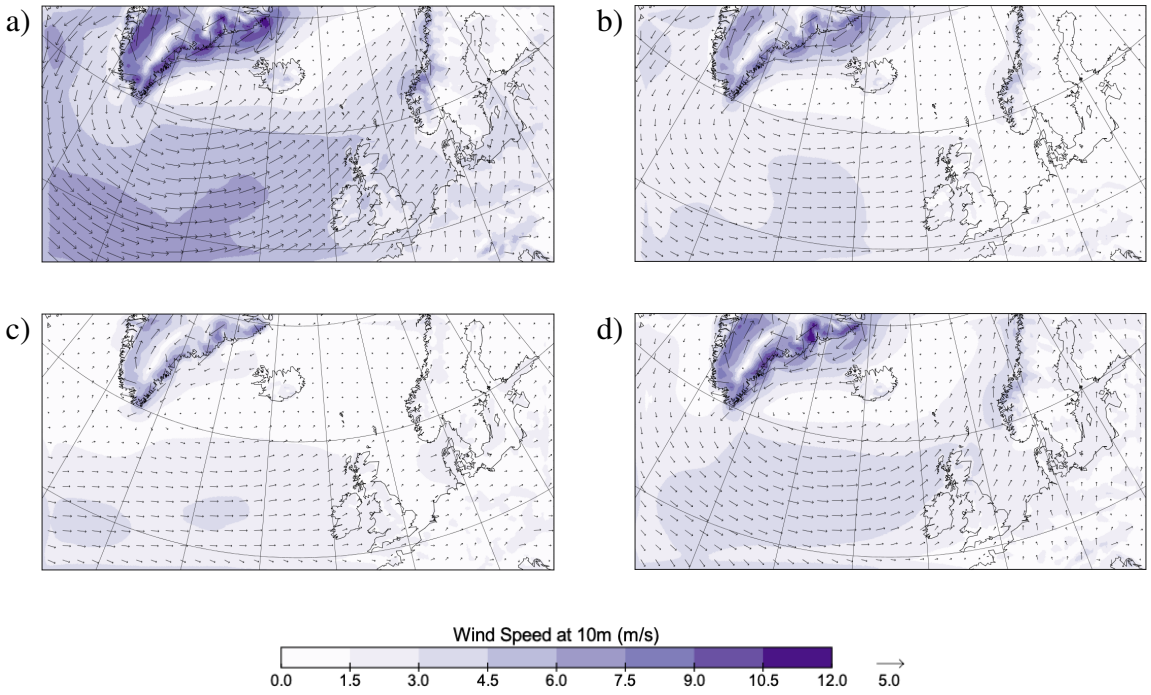

Figure 4.5: Average wind in the control run at 10 m, averaged seasonally for a) winter, b) spring, c) summer, and d) autumn.

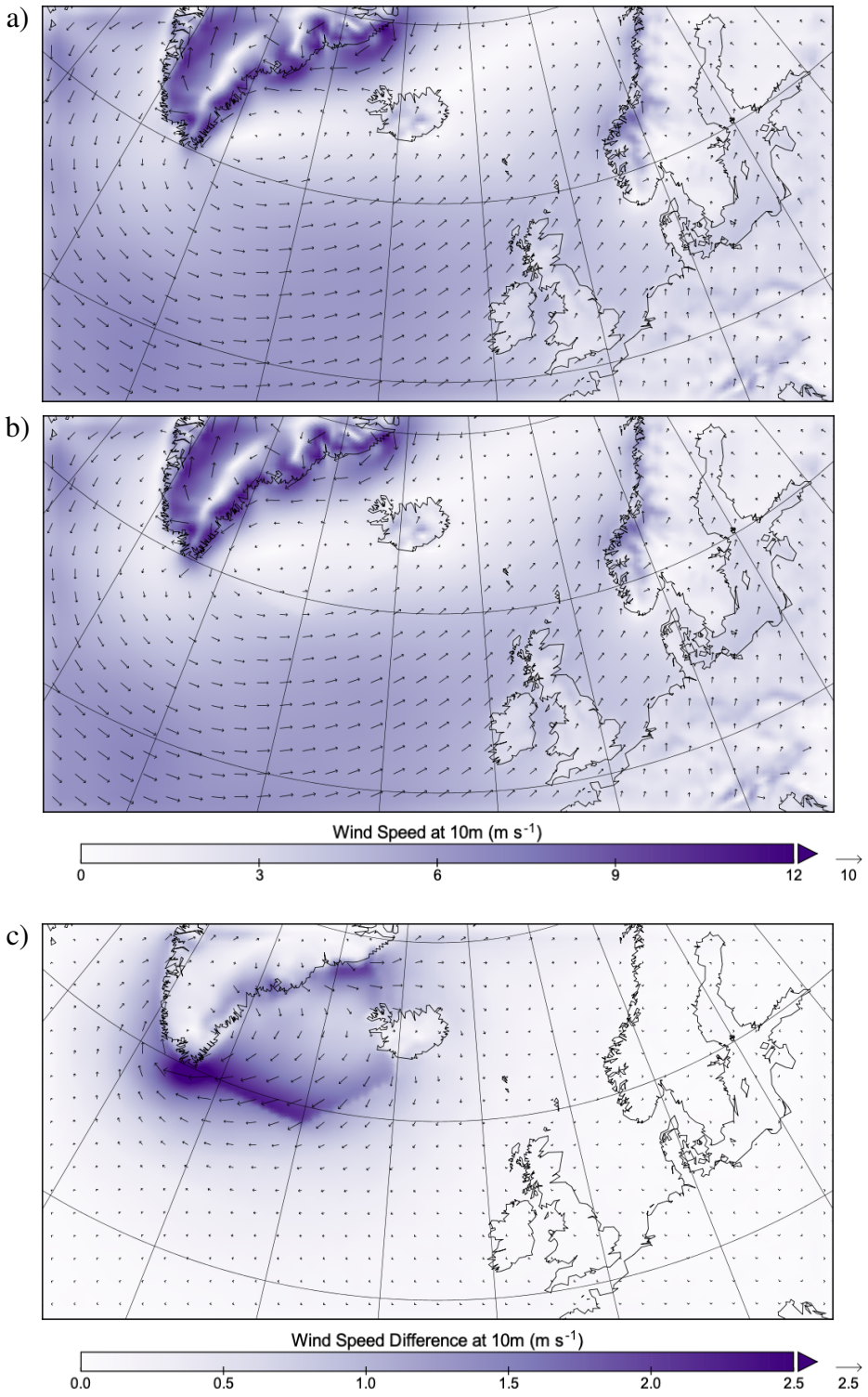

Figure 4.6: (a) Winds in control run at 10 m, averaged seasonally for winter. (b) Winds in experiment run at 10 m, averaged seasonally for winter. (c) Difference between experiment run surface winds and control run surface winds at 10 m, averaged for winter.

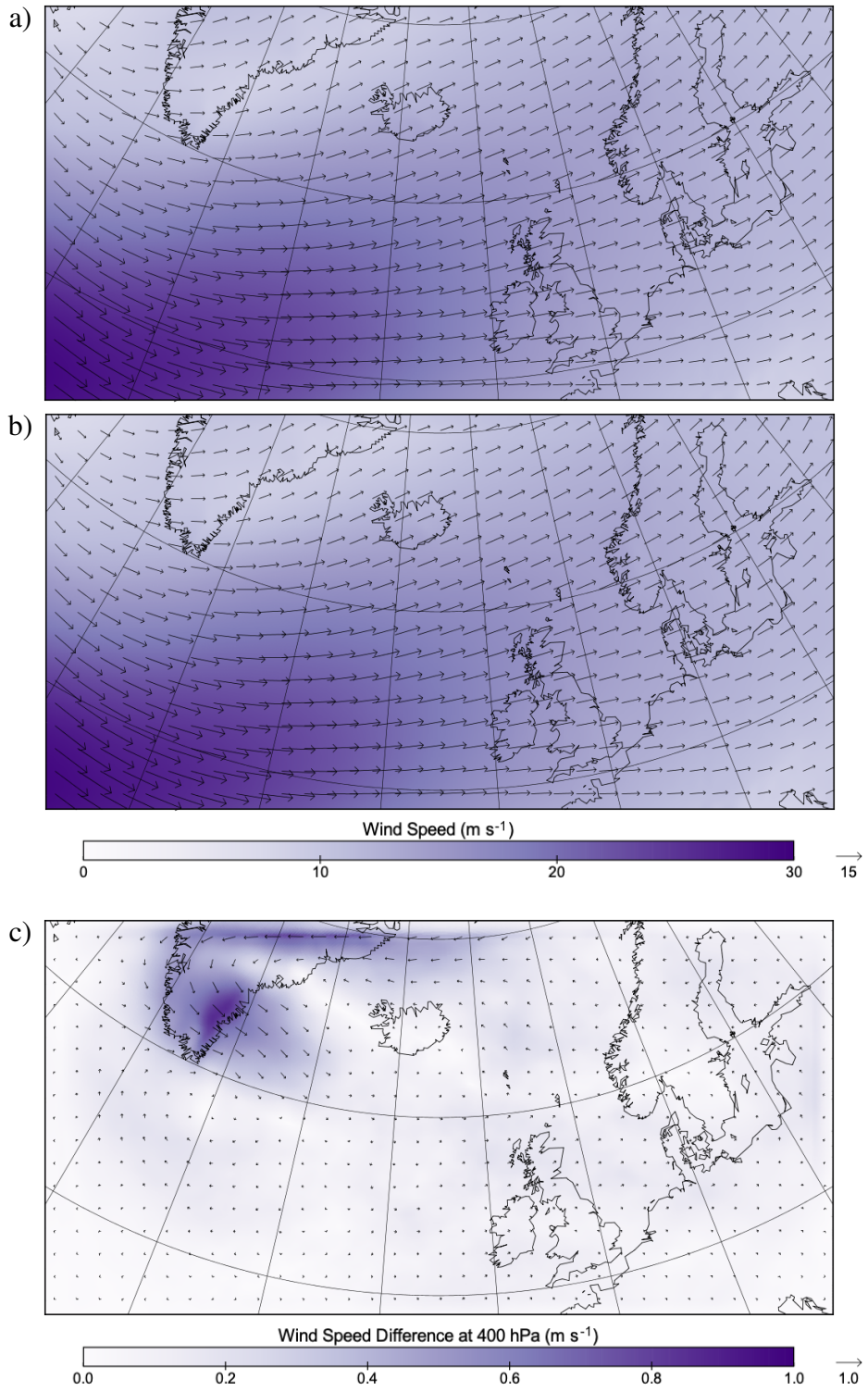

Figure 4.7: (a) Control run wind at 400 hPa, averaged for winter. (b) Experiment run wind at 400 hPa, averaged for winter. (c) Difference between experiment and control runs of wind at 400 hPa for winter. A cyclonic wind difference could be caused by higher temperatures at this height. Similar wind pattern differences exist between 600 hPa and 250 hPa.

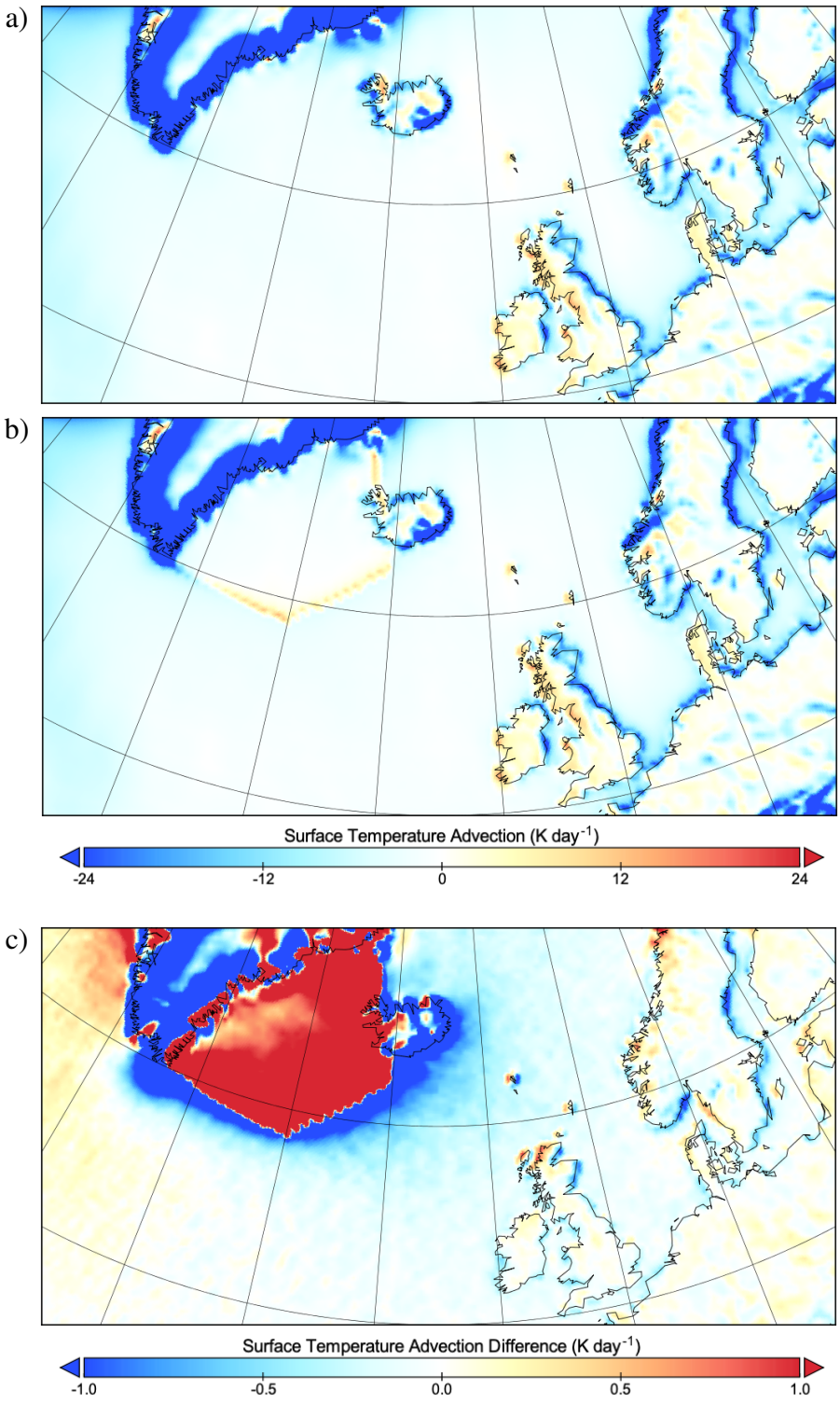

Figure 4.8: (a) Surface air temperature advection in control run, averaged seasonally for winter. (b) Surface air temperature advection in experiment run, averaged seasonally for winter. (c) Difference between experiment run surface air temperature advection and control run surface air temperature advection, averaged for winter. All plots contain noise from the advection calculation algorithm. Scales chosen to show detail over Scandinavia and British Isles.

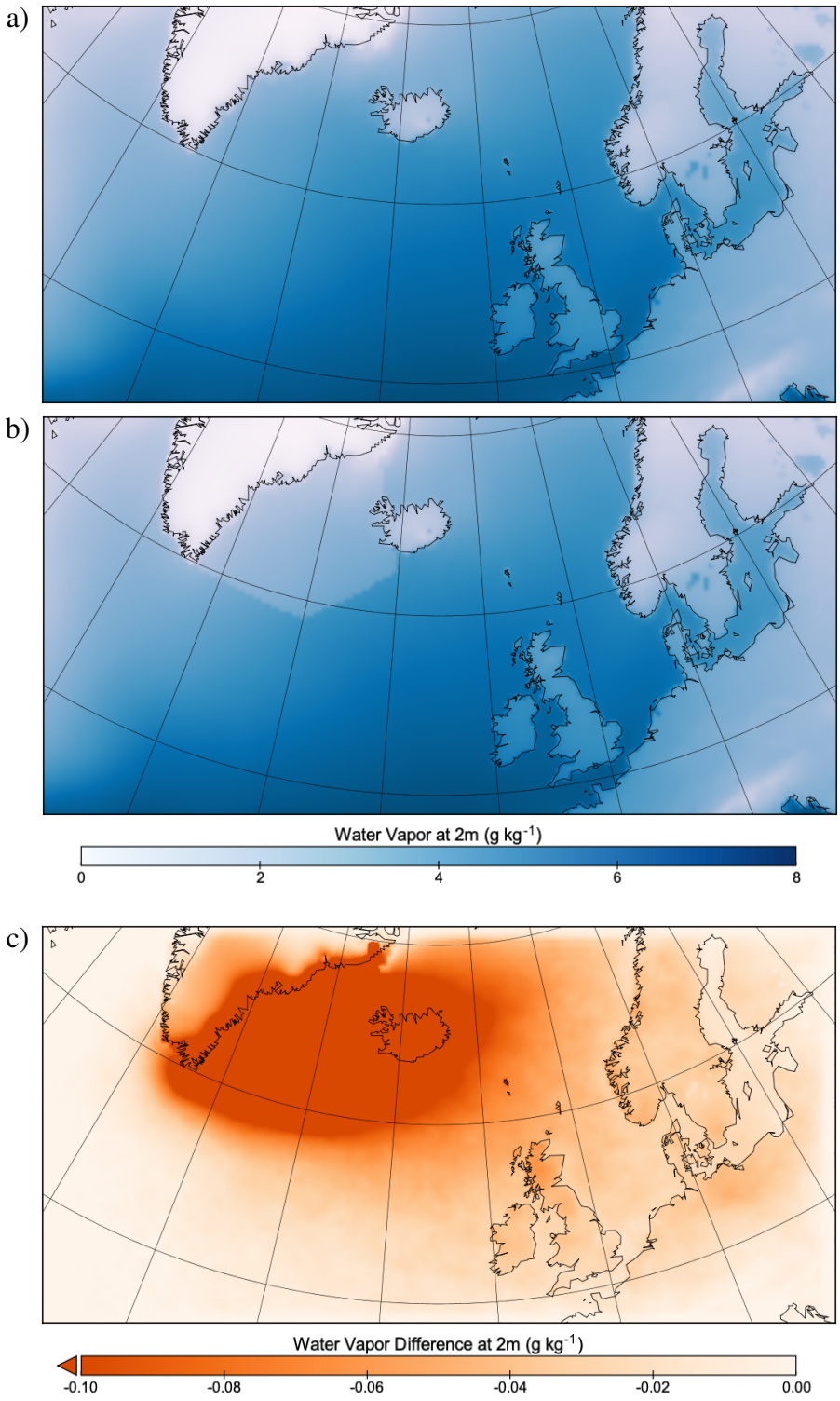

Figure 4.9: (a) Average winter water vapor content at 2 m for control run. (b) Average winter water vapor content at 2 m for experiment run. (c) Water vapor difference between experiment and control runs at 2 m, averaged seasonally for winter. Scales chosen to show detail over Scandinavia and British Isles.

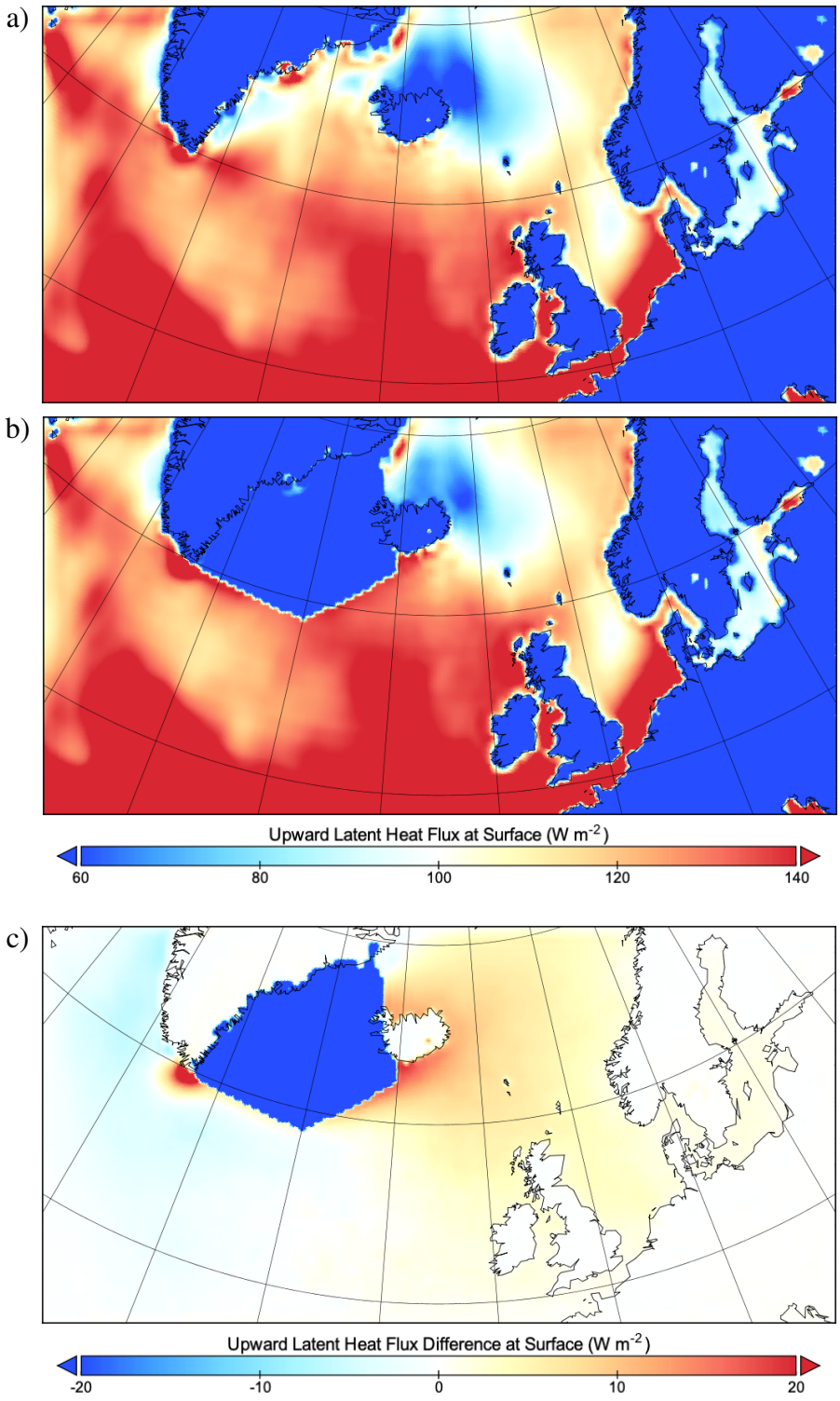

Figure 4.10: (a) Average upward latent heat flux at the surface for control run in winter. (b) Average upward latent heat flux at the surface for experiment run in winter. (c) Difference in upward latent heat flux at the surface between experiment and control runs for winter. Scales chosen to show detail over Norwegian Sea to illustrate effects for Scandinavia and British Isles.

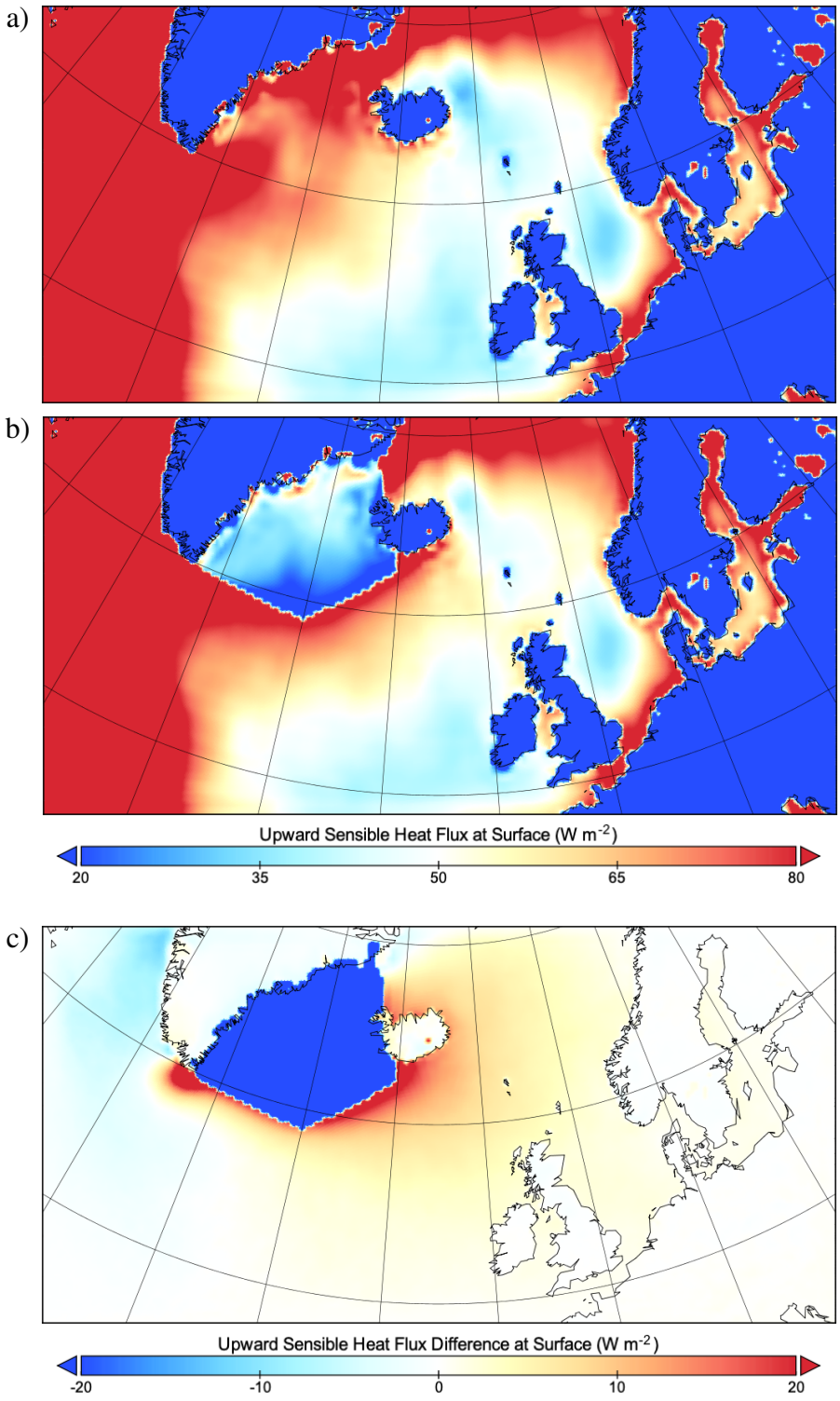

Figure 4.11: (a) Average upward sensible heat flux at the surface for control run in winter. (b) Average upward sensible heat flux at the surface for experiment run in winter. (c) Difference in upward sensible heat flux at the surface between experiment and control runs for winter. Scales chosen to show detail over Norwegian Sea to illustrate effects for Scandinavia and British Isles.

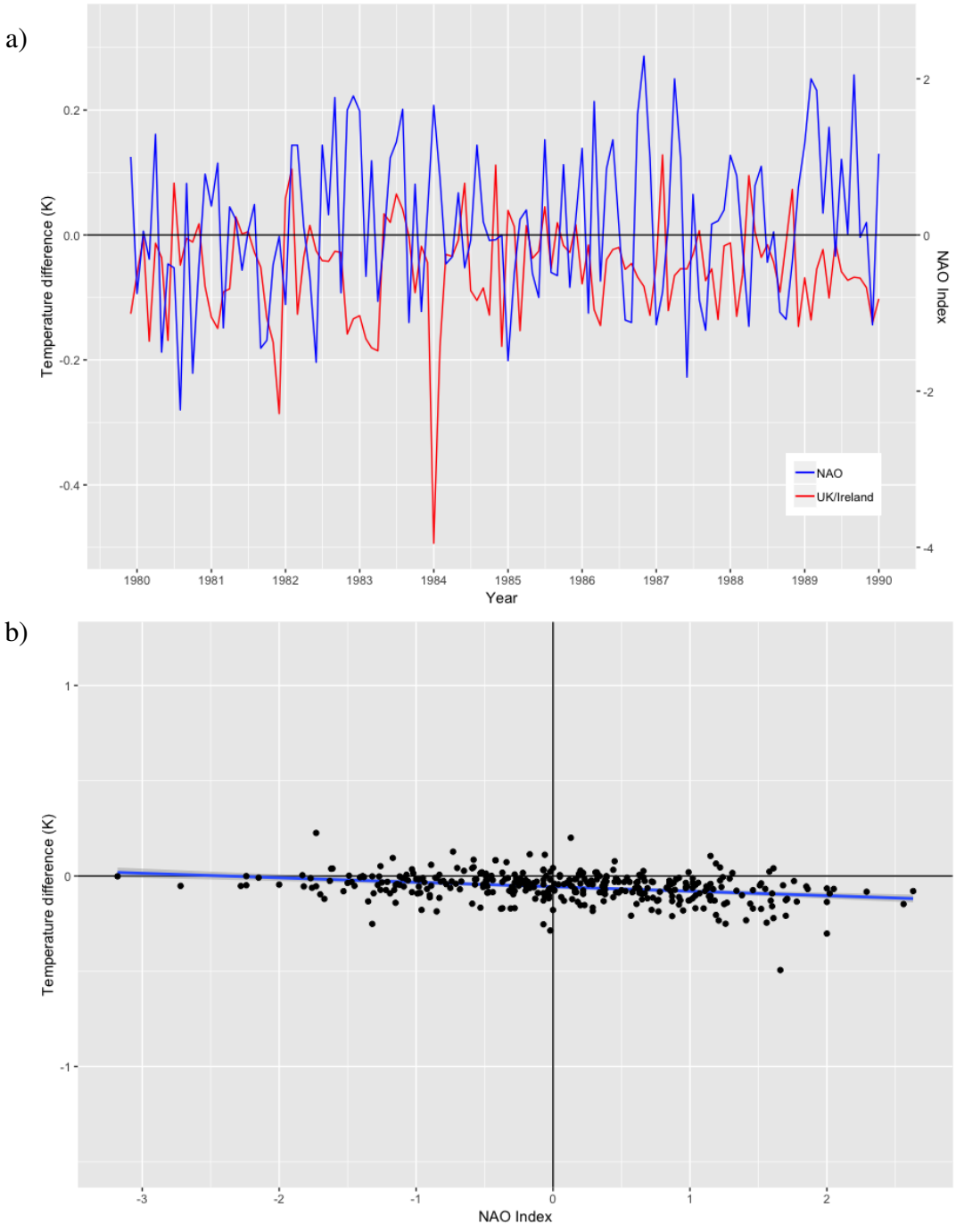

Figure 4.12: (a) 2 m temperature difference between experiment and control runs versus historical NAO index for UK & Ireland study region, for 1979-1990. Other decades of experiment show a similar pattern. (b) Scatter plot for all monthly average data points of the difference between the experiment and control runs, showing relationship between positive NAO and stronger negative temperature difference. Correlated linearly (-0.0236 K change in surface air temperature anomaly per unit increase in NAO) at $R^2 = 0.094$, $p = 1.592 \times 10^{-9}$.

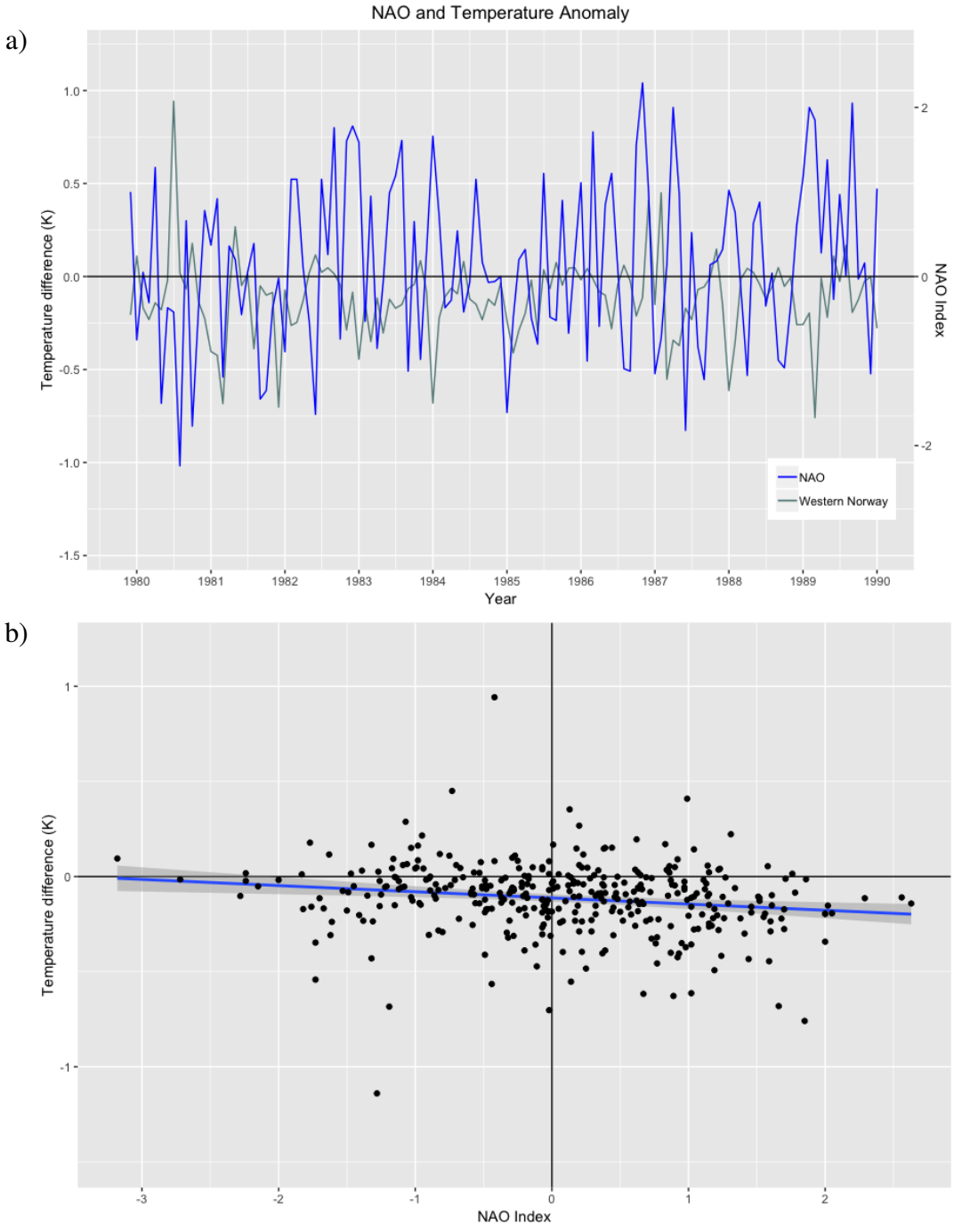

Figure 4.13: (a) 2 m temperature difference between experiment and control runs versus historical NAO index for western Norway study region, for 1979-1990. Other decades of experiment show a similar pattern. (b) Scatter plot for all monthly average data points of the difference between the experiment and control runs, showing relationship between positive NAO and stronger negative temperature difference. Correlated linearly (−0.0325 K change in surface air temperature difference per unit increase in NAO) at $R^2 = 0.026$, $p = 0.0012$.

Table 4.2: Linear correlation statistics between historical NAO index and surface air temperature difference in each study region, for all monthly average data points as well as for each season individually. Slope is given in Kelvins per unit NAO index.

Region		Annual	Winter	Spring	Summer	Autumn
Iceland	slope	-0.1317	-0.1197	-0.1710	-0.0786	-0.1228
	R^2	0.187	0.091	0.213	0.161	0.211
	p	2.2×10^{-16}	2.2×10^{-3}	2.7×10^{-6}	5.2×10^{-5}	3.2×10^{-6}
UK & Ireland	slope	-0.0236	-0.0396	-0.0311	0.0003	-0.0142
	R^2	0.094	0.133	0.129	0.011	0.065
	p	1.592×10^{-9}	2.453×10^{-4}	3.034×10^{-4}	0.9559	8.677×10^{-3}
Ireland	slope	-0.0257	-0.0438	-0.0398	0.0052	-0.0150
	R^2	0.072	0.104	0.149	0.007	0.035
	p	1.534×10^{-7}	1.157×10^{-3}	1.029×10^{-4}	0.5177	4.195×10^{-2}
Scotland	slope	-0.0378	-0.0619	-0.0410	-0.0030	-0.0278
	R^2	0.114	0.178	0.115	0.010	0.104
	p	2.930×10^{-11}	2.054×10^{-5}	6.289×10^{-4}	0.7352	1.158×10^{-3}
Sweden & Norway	slope	-0.0230	-0.0384	-0.0249	0.0114	-0.0145
	R^2	0.036	0.057	0.024	0.007	0.028
	p	1.667×10^{-4}	1.339×10^{-2}	7.891×10^{-2}	0.2101	6.329×10^{-2}
Norway	slope	-0.0296	-0.0407	-0.0221	-0.0040	-0.0207
	R^2	0.040	0.039	0.007	0.010	0.040
	p	8.157×10^{-5}	3.437×10^{-2}	0.2015	0.7246	3.353×10^{-2}
Sweden	slope	-0.0194	-0.0403	-0.0274	0.0232	-0.0111
	R^2	0.026	0.062	0.035	0.060	0.010
	p	1.313×10^{-3}	1.010×10^{-2}	4.358×10^{-2}	1.113×10^{-2}	0.1671
Western Norway	slope	-0.0325	-0.0331	-0.0261	-0.0095	-0.0210
	R^2	0.026	0.009	0.005	0.009	0.019
	p	1.225×10^{-2}	0.1802	0.2388	0.6204	0.1036
Denmark	slope	-0.0137	-0.0206	-0.0060	0.0004	-0.0183
	R^2	0.011	0.009	0.009	0.011	0.064
	p	2.366×10^{-2}	0.1797	0.6733	0.9712	9.437×10^{-3}

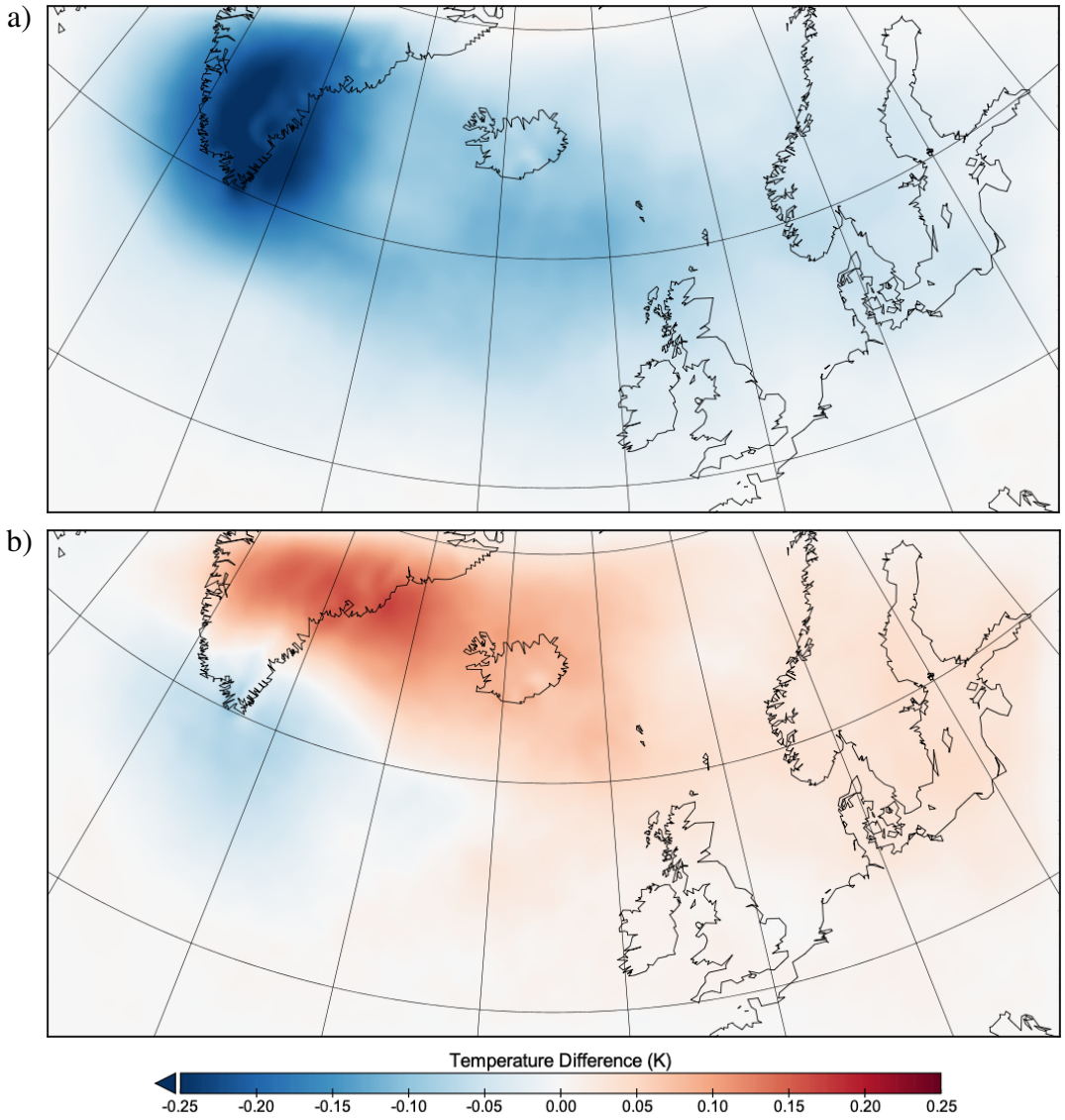

Figure 4.14: (a) 500 hPa temperature difference between experiment and control runs, averaged for winter. The center of the temperature difference has shifted to the west of the SST anomaly. (b) 300 hPa temperature difference between experiment and control runs, averaged for winter. A positive temperature anomaly above Greenland and Iceland indicates a slight lowering of the tropopause. The temperature pattern fits with the wind difference at this level of the atmosphere (see also Fig. 4.7).

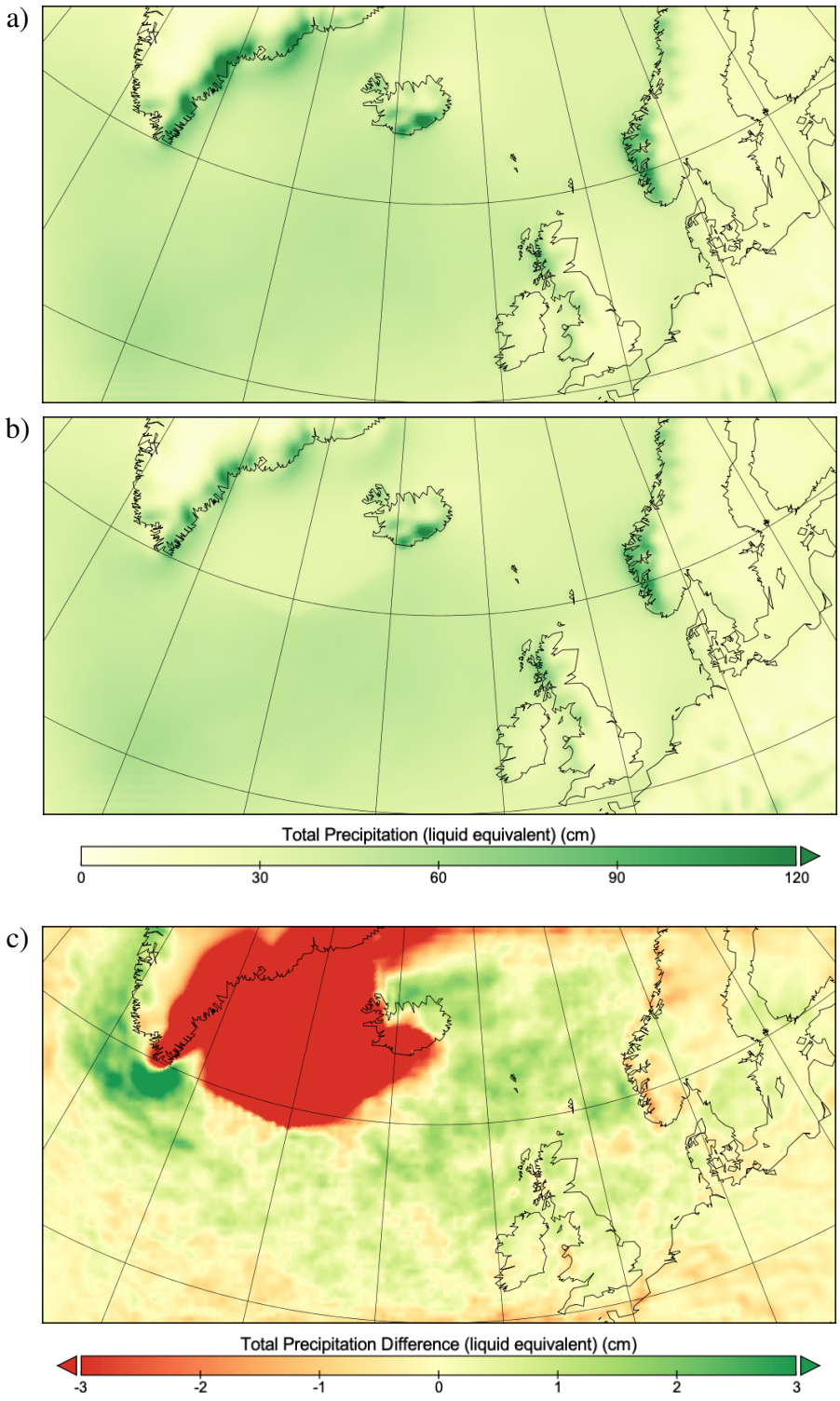

Figure 4.15: (a) Control run liquid equivalent of total precipitation, averaged for winter. Values scaled to a 90-day season by dividing the total precipitation in the season by the number of days in the season, then multiplying by 90. (b) Experiment run liquid equivalent of total precipitation, averaged for winter. Values calculated as with (a). (c) Liquid equivalent of total precipitation difference between experiment and control runs for winter. Values scaled to a 90-day season as with (a). Scales chosen to show detail over Scandinavia and British Isles.

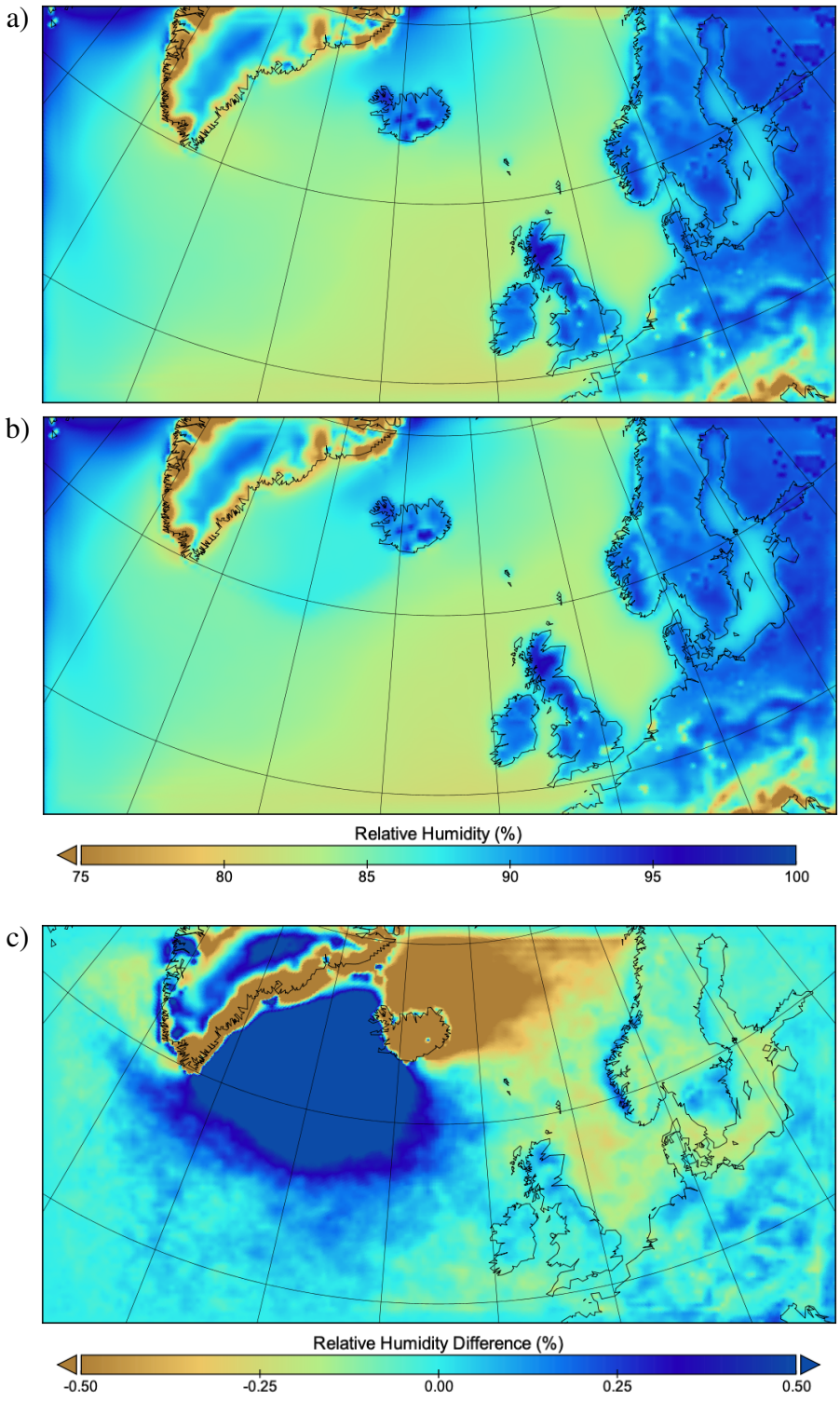

Figure 4.16: (a) Relative humidity at 2 m for control run, averaged for winter. (b) Relative humidity at 2 m for experiment run, averaged for winter. (c) Relative humidity difference between experiment and control run at 2 m, averaged seasonally for winter. Relative humidity difference was calculated by computing relative humidity for the control and experiment runs, and then subtracting the percentage value of the control run from that of the experiment run. Scales chosen to show detail over Scandinavia and British Isles.

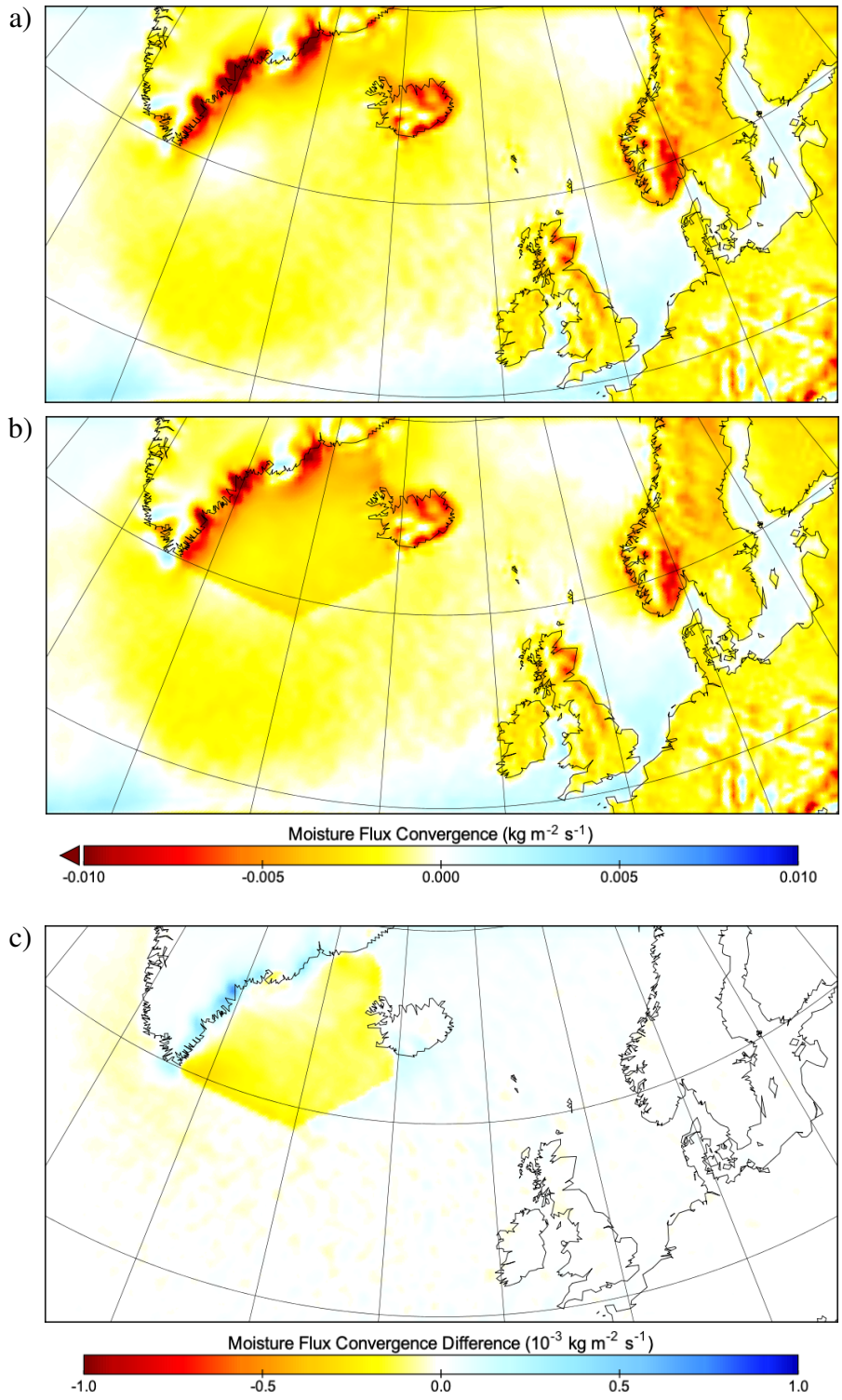

Figure 4.17: (a) Control run vertically integrated moisture flux convergence, averaged for winter. Moisture flux convergence was integrated from 1000 hPa to 100 hPa. (b) Experiment run vertically integrated moisture flux convergence, averaged for winter. Values calculated as with (a). Both (a) and (b) contain noise from the gradient calculation algorithm. Scales for (a) and (b) were chosen to show detail over Scandinavia and British Isles. (c) Total vertically integrated moisture flux convergence difference between experiment and control runs for winter. Scale for (c) chosen to eliminate noise from gradient calculation algorithm.

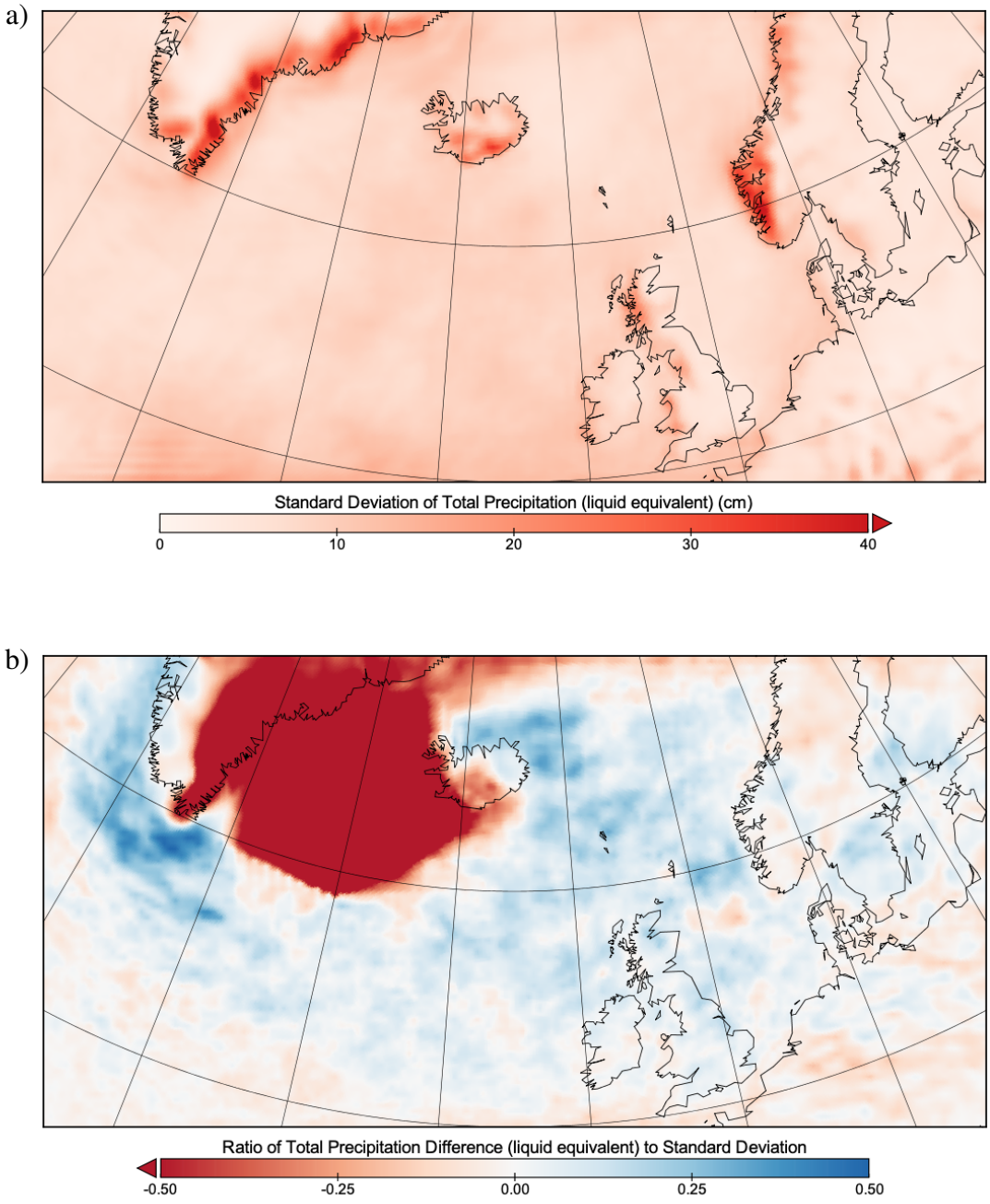

Figure 4.18: (a) Standard deviation between average winter liquid equivalent of total precipitation for each year in control run. (b) Ratio of liquid equivalent of total precipitation difference to standard deviation between average winter liquid equivalent of total precipitation. Scales chosen to show detail over Scandinavia and British Isles.

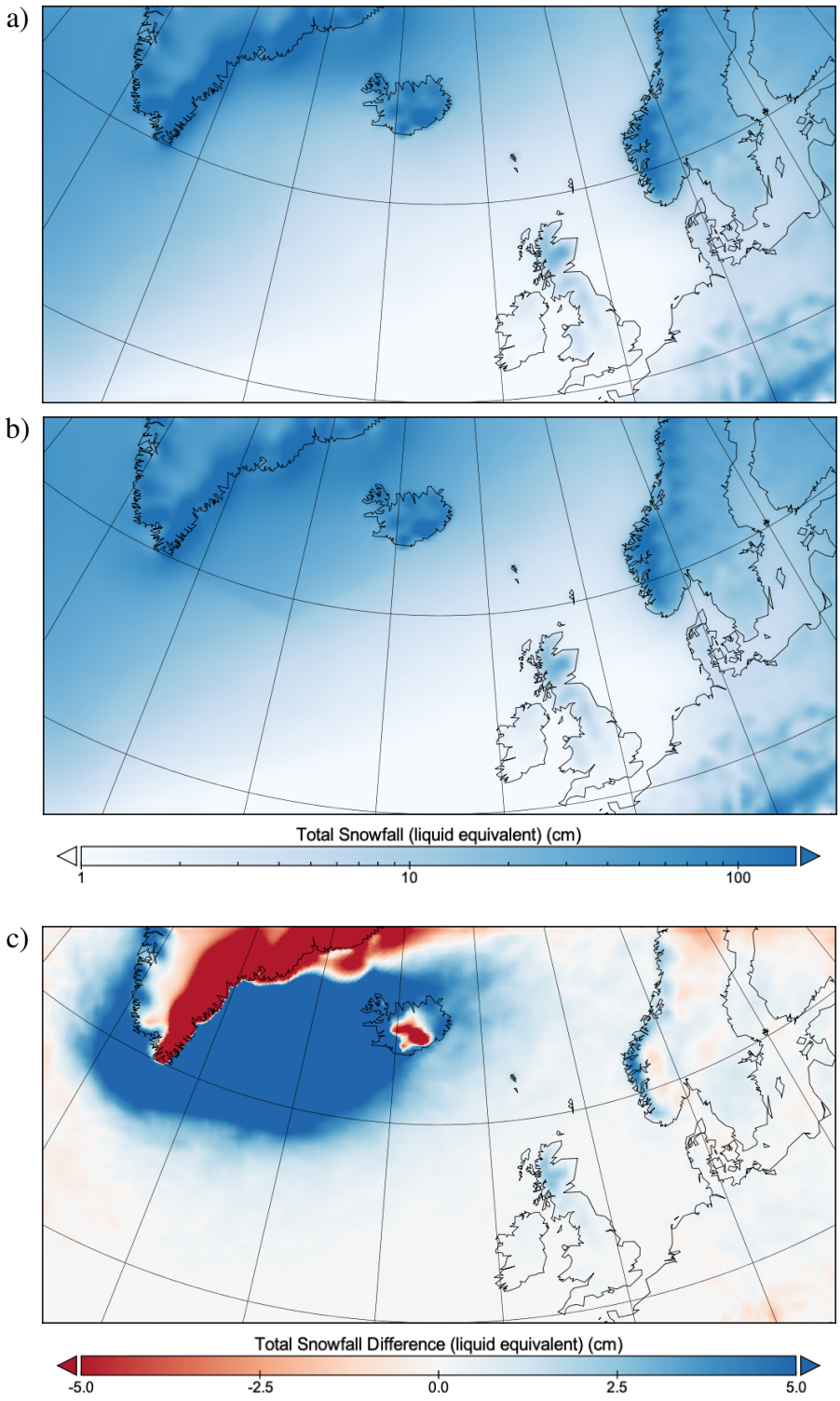

Figure 4.19: (a) Average yearly liquid equivalent of total snowfall in control run, on a logarithmic scale. (b) Average yearly liquid equivalent of total snowfall in experiment run, on a logarithmic scale. (c) Difference of average yearly liquid equivalent of total snowfall between experiment and control runs, on a linear scale. Scales chosen to show detail over Scandinavia and British Isles.

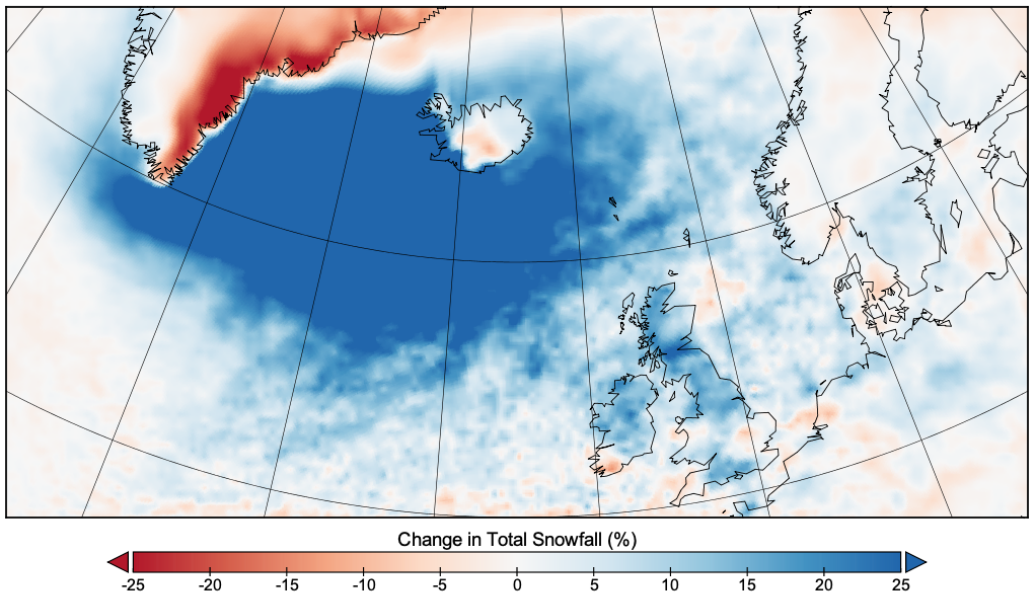

Figure 4.20: Percent change of average yearly total snowfall in experiment run compared to control run. Scale chosen to show detail over Scandinavia and British Isles.

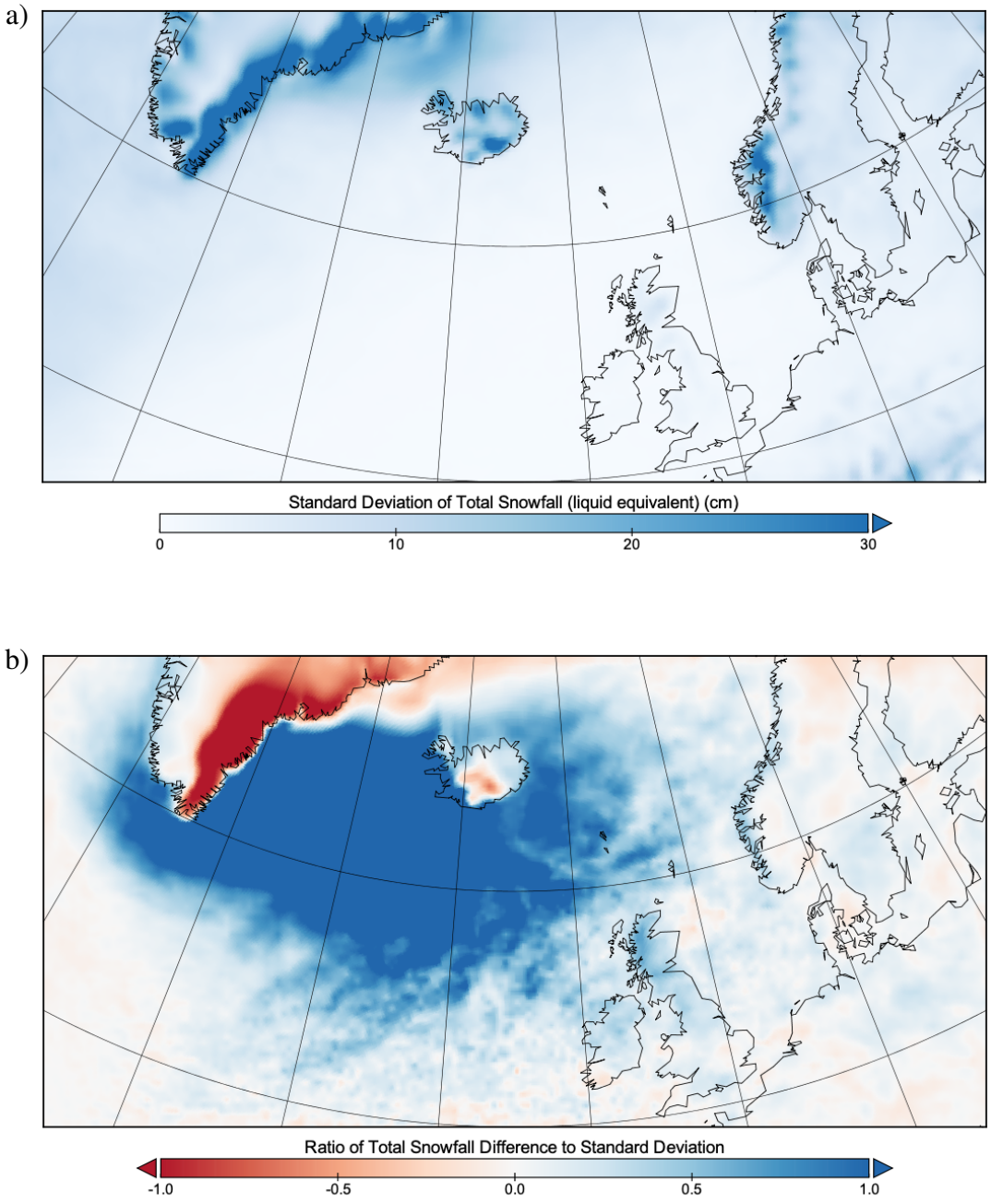

Figure 4.21: (a) Standard deviation between average winter liquid equivalent of total snowfall for each year in control run. (b) Ratio of liquid equivalent of total snowfall difference to standard deviation between average winter liquid equivalent of total snowfall for the control run. Scales chosen to show detail over Scandinavia and British Isles.

Chapter 5

Summary & Conclusion

It is well established that the Atlantic Meridional Overturning Circulation (AMOC) is responsible for keeping Scandinavia and the British Isles relatively warm for their high latitudes, by transporting heat from the tropics to the North Atlantic. However, climate change is causing the Greenland Ice Sheet (GrIS) to melt, which injects freshwater into the path of AMOC and slows it. The results displayed in this thesis show that if enough of GrIS melted and AMOC slowed down enough to impart a $-5\,\mathrm{K}$ sea surface temperature (SST) anomaly in an area between Greenland and Iceland, the resulting climate in Scandinavia and the British Isles would be $\sim 0.15\,\mathrm{K}$ cooler during the winter. This effect would be present yet not as strong during the spring, summer, and fall months. This effect was also found to be correlated with the North Atlantic Oscillation (NAO) index, as a positive NAO would invoke stronger westerly winds which would blow cooler air above the SST anomaly to the study regions.

The change to the sea surface temperature near Greenland would produce other effects for Scandinavia and the British Isles beyond surface air temperature changes. The SST anomaly would drive an increase in relative humidity for these areas which would lead to a slight increase in precipitation for some areas. The British Isles, and particularly Scotland, would experience a greater proportion of their precipitation as snowfall due to

temperature differences, and would see a 5–20% increase in yearly snowfall. Precipitation in Scandinavia would be less affected, mostly because of the distance of this region from the SST anomaly and the topography of mountainous western Norway. The total amount of precipitation received by the region would not be appreciably affected.

This experiment is highly theoretical in nature. The method of applying the SST anomaly to a large region near Greenland was used to emulate the effect of AMOC slowdown from GrIS melting, and to attempt to isolate the atmospheric effects of this change on Scandinavia and the British Isles from any other effects. However, should AMOC slow down, the changes to the ocean-atmosphere system would not be isolated to a mere SST decrease in a single region. A large portion of AMOC overturning occurs in the Labrador Sea to the southwest of Greenland, so there would likely be sea surface temperature differences there as well. With less heat transported northward from the equator via AMOC, it is likely that the entire North Atlantic would be colder at the surface, both in the ocean and the atmosphere. The difference would likely be on the order of 1–2 K, as seen via the "cold blob" phenomenon. In that vein, a decrease of 5 K in sea surface temperature around Greenland is unlikely. Even if enough heat were removed from the region to impact the temperature of the area of the SST anomaly that much, mixing in the North Atlantic would spread this effect out among all the waters in the model domain and more. Finally, the use of WRF without the ocean component in this research poses a problem: since sea surface temperatures are prescribed by the input, we cannot analyze the sensible heat transfer between the anomaly and the waters surrounding it. This led to some simulation output which was unrealistic; for example, the experiment run contained much cooler air than the control run, above water outside the SST anomaly that was the same temperature as that in the control run. In reality, there would be more feedback and evening out of temperatures between the sea surface and the surface air. However, the experiment serves to show how cooler surface temperatures from AMOC slowdown and GrIS melting would propagate to Scandinavia and the British Isles, and illustrates the effects of such a propagation to a finer degree than global climate

models.

This experiment could serve as a base for further research into the impacts of GrIS melting and AMOC slowdown. Other experiments could build off of this one by utilizing SST anomalies of $-2.5\,\mathrm{K}$, $-7.5\,\mathrm{K}$, and $-10.0\,\mathrm{K}$ to quantify the linearity of the effect. Different shapes of the SST anomaly and gradients of its strength within could serve to provide a more realistic simulation. However, the most impactful expansion of this experiment might be running it forced by data from future global emissions scenarios. By doing this, researchers could examine this effect in the context of global warming (which, indeed is the examined cause of the phenomenon through GrIS melting) and find the feedbacks and linkages within. Combined with the spectrum of research into changes of AMOC strength over the next century, this research could aid in giving complete climatologies under various situations for Scandinavaia and the British Isles.

References

Bakker, P., and Coauthors, 2016: Fate of the Atlantic Meridional Overturning Circulation: Strong decline under continued warming and Greenland melting. *Geophysical Research Letters*, **43 (23)**, 12,252–12,260, doi:10.1002/2016GL070457.

Blaschek, M., P. Bakker, and H. Renssen, 2015: The influence of Greenland ice sheet melting on the Atlantic meridional overturning circulation during past and future warm periods: a model study. *Climate Dynamics*, **44 (7-8)**, 2137–2157, doi:10.1007/s00382-014-2279-1.

Bryden, H. L., and S. Imawaki, 2001: Ocean heat transport. *International Geophysics*, **77**, 455–474.

Bryden, H. L., H. R. Longworth, and S. A. Cunningham, 2005: Slowing of the Atlantic meridional overturning circulation at 25 degrees N. *Nature*, **438**, 655–657, doi:10.1038/nature04385.

Caesar, L., S. Rahmstorf, A. Robinson, G. Feulner, and V. Saba, 2018: Observed fingerprint of a weakening Atlantic Ocean overturning circulation. *Nature*, **556 (7700)**, 191–196, doi:10.1038/s41586-018-0006-5.

Cheng, W., J. C. H. Chiang, D. Zhang, W. Cheng, J. C. H. Chiang, and D. Zhang, 2013: Atlantic Meridional Overturning Circulation (AMOC) in CMIP5 Models: RCP and Historical Simulations. *Journal of Climate*, **26 (18)**, 7187–7197, doi:10.1175/JCLI-D-12-00496.1.

Church, J., J. Gregory, and Coauthors., 2001: Changes in Sea Level. *Climate Change 2001: The Scientific Basis*, 639–694.

Curry, R., 2010: North Atlantic portion of the Atlantic Meridional Overturning Circulation. URL http://editors.eol.org/eoearth/wiki/File:OCP07_Fig-6.jpg, online; accessed May 13, 2019.

Danabasoglu, G., S. G. Yeager, Y.-O. Kwon, J. J. Tribbia, A. S. Phillips, and J. W. Hurrell, 2012: Variability of the Atlantic Meridional Overturning Circulation in CCSM4. *Journal of Climate*, **25 (15)**, 5153–5172, doi:10.1175/JCLI-D-11-00463.1.

Driesschaert, E., and Coauthors, 2007: Modeling the influence of Greenland ice sheet melting on the Atlantic meridional overturning circulation during the next millennia. *Geophysical Research Letters*, **34 (10)**, 1–5, doi:10.1029/2007GL029516.

Duchez, A., and Coauthors, 2014: A New Index for the Atlantic Meridional Overturning Circulation at 26°N. *Journal of Climate*, **27 (17)**, 6439–6455, doi:10.1175/JCLI-D-13-00052.1.

Frajka-Williams, E., J. Bamber, and K. Våge, 2016: Greenland Melt and the Atlantic Meridional Overturning Circulation. *Oceanography*, **29 (4)**, 22–33, doi:10.5670/oceanog.2016.96.

Frajka-Williams, E., and Coauthors, 2019: Atlantic Meridional Overturning Circulation: Observed Transport and Variability. *Frontiers in Marine Science*, **6**, 260, doi:10.3389/fmars.2019.00260.

Hansen, J., M. Sato, P. Kharecha, G. Russell, D. W. Lea, and M. Siddall, 2007: Climate change and trace gases. *Philosophical Transactions of the Royal Society A: Mathematical, Physical and Engineering Sciences*, **365 (1856)**, 1925–1954, doi:10.1098/rsta.2007.2052.

Hassol, S. J., 2004: Impacts of a Warming Arctic. Tech. rep., Arctic Climate Impact Assessment.

Hu, A., G. A. Meehl, W. Han, and J. Yin, 2009: Transient response of the MOC and climate to potential melting of the Greenland Ice Sheet in the 21st century. *Geophysical Research Letters*, **36 (10)**, 1–6, doi:10.1029/2009GL037998.

IPCC, 2013: *Climate Change 2013: The Physical Science Basis. Contribution of Working Group I to the Fifth Assessment Report of the Intergovernmental Panel on Climate Change*. Cambridge University Press, Cambridge, United Kingdom and New York, NY, USA, 1535 pp., doi:10.1017/CBO9781107415324.

Liu, W., S.-P. Xie, Z. Liu, and J. Zhu, 2017: Overlooked possibility of a collapsed Atlantic Meridional Overturning Circulation in warming climate. *Science Advances*, **3 (1)**, e1601 666, doi:10.1126/sciadv.1601666.

Rahmstorf, S., J. Box, G. Feulner, M. E. Mann, A. Robinson, S. Rutherford, and E. Schaffernicht, 2015: Evidence for an exceptional twentieth-century slowdown in Atlantic Ocean overturning. *Nature Climate Change*, **5 (10)**, 475–480, doi:10.1038/nclimate2781.

Rossby, T., 1996: The north atlantic current and surrounding waters: At the crossroads. *Reviews of Geophysics*, **34**, 463–481.

Saha, S., and Coauthors, 2010: NCEP Climate Forecast System Reanalysis (CFSR) 6-hourly Products, January 1979 to December 2010. Research Data Archive at the National Center for Atmospheric Research, Computational and Information Systems Laboratory, Boulder CO, [Available online at https://doi.org/10.5065/D69K487J.] Accessed 27-04-2018.

Seager, R., D. S. Battisti, J. Yin, N. Gordon, N. H. Naik, A. C. Clement, and M. A. Cane, 2002: Is the Gulf Stream responsible for Europe's mild winters? *Quarterly Journal of the Royal Meteorological Society*, **128**, 2563–2586.

Sévellec, F., A. V. Fedorov, and W. Liu, 2017: Arctic sea-ice decline weakens the Atlantic Meridional Overturning Circulation. *Nature Climate Change*, **7 (8)**, 604–610, doi:10.1038/nclimate3353.

Skamarock, W., and Coauthors, 2008: A description of the Advanced Research WRF version 3. NCAR Tech. Note NCAR/TN-475+STR, 113 pp. [doi:10.5065/D68S4MVH].

Thornalley, D. J. R., and Coauthors, 2018: Anomalously weak Labrador Sea convection and Atlantic overturning during the past 150 years. *Nature*, **556 (7700)**, 227–230, doi: 10.1038/s41586-018-0007-4.

Vellinga, M., and R. A. Wood, 2002: Global climatic impacts of a collapse of the Atlantic thermohaline circulation. *Climatic Change*, **54 (3)**, 251–267, doi: 10.1023/A:1016168827653.

Wallace, J. M., and P. V. Hobbs, 2006: *Atmospheric Science: An Introductory Survey*. Academic Press, 483 pp.

Yu, L., Y. Gao, and O. H. Otterå, 2016: The sensitivity of the Atlantic meridional overturning circulation to enhanced freshwater discharge along the entire, eastern and western coast of Greenland. *Climate Dynamics*, **46 (5-6)**, 1351–1369, doi:10.1007/s00382-015-2651-9.